Inconsistency in spatial distributions and temporal trends derived from nine operational global aerosol optical depth products

Jing Wei[1,2], Yiran Peng[1*], Rashed Mahmood[3], Lin Sun[4], Jianping Guo[5]

[1] Ministry of Education Key Laboratory for Earth System Modeling, Department of Earth System Science, Tsinghua University, Beijing, China
[2] State Key Laboratory of Earth Surface Processes and Resource Ecology, College of Global Change and Earth System Science, Beijing Normal University, Beijing, China
[3] Department of Atmospheric Science, School of Environmental Studies, China University of Geosciences, Wuhan, China
[4] College of Geomatics, Shandong University of Science and Technology, Qingdao, China
[5] State Key Laboratory of Severe Weather, Chinese Academy of Meteorological Sciences, Beijing, China

Correspondence to: Yiran Peng (pyiran@mail.tsinghua.edu.cn)

Abstract

Satellite-derived aerosol products provide long-term and large-scale observations for analysing aerosol distributions and variations, climate-scale aerosol simulations, and aerosol-climate interactions. Therefore, a better understanding of the consistencies and differences among multiple aerosol products is of great importance. The objective of this study is to evaluate nine operational global aerosol optical depth (AOD) products, including the European Space Agency Climate Change Initiative (ESA-CCI) Advanced Along-Track Scanning Radiometer (AATSR), Advanced Very High Resolution Radiometer (AVHRR), Multi-angle Imaging Spectro Radiometer (MISR), Moderate Resolution Imaging Spectroradiometer (MODIS), and Sea-Viewing Wide Field-of-View Sensor (SeaWiFS) over the land and oceans during the period from 1997 to 2017. Aerosol Robotic Network (AERONET) Version 3 Level 2.0 (cloud screened and quality assured) measurements at 243 sites around the world are selected for validation purposes. Our results illustrate that noticeable inconsistencies exist in spatial coverages, variations, and temporal trends among different aerosol products. Large annual mean AOD differences greater than 0.15 are mainly found in North Africa, Central Africa, the Middle East, and East Asia, as well as in the coastal areas of western North America and Asia. In general, the AATSR Swansea University (SU) product appears to have the best accuracy, the SeaWiFS product obviously underestimates aerosol loadings over the land and ocean, and the MODIS products seriously overestimate aerosol loadings over the land and ocean. For temporal trends, more than 77% and 72% of land and ocean sites, respectively, show the same trends direction as the ground observations. However, numerical differences are non-negligible in North Africa, the Middle East, and South Asia and in most open oceans. MODIS products are generally

more accurate in describing the temporal trends over the land and ocean. The aerosol loadings trend changed from positive to negative over the past two decades (2000-2017) in some continental areas. These results suggest that multiple AOD products

35   show significant numerical inconsistencies in describing spatial distributions and temporal trends, which should be carefully considered when users choose aerosol products for their studies.

1 Introduction

Atmospheric aerosols originating from both natural and anthropogenic sources have noticeable effects on the ecological

40   environment, climate change, urban air quality and human health; these issues are also attracting increasing attention from national governments and scientists (Cao et al., 2012; Guo et al., 2016, 2017; Li et al., 2011; Li et al., 2017; Pöschl, 2005). On the one hand, the enhanced anthropogenic aerosols in the past century have significantly affected the radiation budget balance by scattering or absorbing solar radiation and by changing cloud microphysical properties (Ramanathan et al., 2001; Rosenfeld et al., 2008). On the other hand, fine particulate matter greatly endangers human health by causing various

45   respiratory and cardiovascular diseases (Brauer et al., 2012; Bartell et al., 2013; Crouse et al., 2012). However, due to the complex sources, compositions and short lifetimes of atmospheric aerosols, large uncertainties exist in the estimation of aerosol-climate forcings and health effects. To better understand the spatial and temporal variability of aerosol distributions from regional to global scales, long-term data records with reasonable accuracy are needed as benchmarks to evaluate aerosol effects based on climate model simulations.

50   Since the 19th century, several aerosol ground-based observation networks, such as the worldwide Aerosol Robotic Network (AERONET), Interagency Monitoring of Protected Visual Environments (IMPROVE), European Monitoring and Evaluation Programme (EMEP), and Chinese Sun Hazemeter Network (CSHNET), have been established. Monitoring stations are sparsely distributed, and the observation periods at different sites vary across a large range due to instrumental or weather conditions. Therefore, ground-based observational data are limited in representing aerosol characteristics in long-term and

55   large-scale studies. Since the 1990s, the continuous launch of satellite sensors has enabled the satellite aerosol remote sensing, which provides long-term data records with wide spatial coverage. Meanwhile, an abundance of mature aerosol retrieval algorithms have been developed according to the observable characteristics of different satellite sensors and of atmospheric radiative transfer models, and these algorithms have been successfully applied to generate global-coverage aerosol products for over 10 years. These satellite instruments include the Advanced Very High Resolution Radiometer

60   (AVHRR), Total Ozone Mapping Spectrometer (TOMS), Advanced Along-Track Scanning Radiometer (AATSR), Multi-angle Imaging Spectro Radiometer (MISR), Moderate Resolution Imaging Spectroradiometer (MODIS), Sea-Viewing Wide Field-of-View Sensor (SeaWiFS) and Cloud-Aerosol Lidar with Orthogonal Polarization (CALIPSO).

Based on these long-term space-borne aerosol products, numerous researchers have begun to explore aerosol spatial and temporal variations at regional and global scales as well as the potential climate effects of aerosols. For example, Guo et al.

65 (2011) analysed the temporal and spatial distributions and trends in Aerosol Optical Depth (AOD) over eight typical regions in China by combining TOMS (1980–2001) and MODIS (2000–2008, Collection 5.1) aerosol products. Hsu et al. (2012) explored the global and regional AOD trends over the land and oceans from 1997 to 2010 based on the SeaWiFS monthly aerosol products. Zhao et al. (2013) analysed the AVHRR AOD datasets over the global oceans and explored the effects of subpixel cloud contamination on aerosol retrievals from 1981 to 2009. Mehta et al. (2016) presented the spatiotemporal

70 AOD variations and their spatial correlations globally and over six subregions using the MODIS (Collection C5.1) and MISR monthly products from 2001 to 2014. He et al. (2016) investigated spatiotemporal AOD variations and analysed several main indices influencing the aerosol variation in China and five typical regions using MODIS (Collection 6) aerosol products from 2002-2015. Klingmüller et al. (2016) studied aerosol trends over the Middle East and explored the effects of rainfall, soil moisture and surface winds on aerosols with MODIS (Collection 6) aerosol products from 2000 to

75 2015. Sogacheva et al. (2018) discussed the spatial and seasonal variations of aerosols over China based on two decades of multisatellite observations using AATSR (1995–2012) and MODIS (2000–2017, Collection 6.1) aerosol products.

In most of the above studies, satellite-derived aerosol products are arbitrarily selected for research applications, simply following the usage in previous studies or based on data availability. However, noticeable inconsistencies exist among the aerosol datasets generated from different satellite sensors and aerosol retrieval algorithms. Seemingly, few studies have

80 focused on exploring the similarities and differences among aerosol datasets. Choosing an accurate and appropriate aerosol product to represent long-term aerosol variations and trends for their respective studies is of great importance for users, especially interdisciplinary scholars. Otherwise, problematic aerosol characteristics will inevitably lead to questionable conclusions.

The objective of this study is to comprehensively investigate the consistencies and differences in aerosol characteristics

85 among multiple operational global aerosol products from satellites. For evaluations and comparisons, a total of nine aerosol products with the most up-to-date versions are selected in this paper, including the European Space Agency's Climate Change Initiative (CCI) products AATSR-Dual View (ADV), AATSR Swansea University (SU), AATSR-Oxford-RAL Retrieval of Aerosol and Cloud (ORAC) and AATSR-ENSEMBLE, which cover the period of 1996-2012, and the MISR (2000~2017), Terra (2000~2017), Aqua (2002~2017) MODIS, SeaWiFS (1997~2010) and AHVRR (1997~2017) products.

90 AERONET ground-based AOD measurements at 243 globally distributed sites over the land and oceans are collected for validations.

This study is organized as follows: a description of nine satellite global aerosol products and AERONET data sources is provided in Section 2. In Section 3, the matching method for validation, calculation approaches for aerosol distributions and trends, and quantitative evaluation metrics are presented. The statistical evaluation results for monthly AOD retrieval are

95 presented in Section 4. In Section 5, the regional and global AOD distributions are analysed, and a comparison of aerosol trends and their specific features during the last two decades are provided in Section 6. A brief summary and conclusion are given in the final section.

2 Data description

2.1 Operational aerosol products

2.1.1 ESA-CCI aerosol products

100 Four typical ESA-CCI (Hollmann et al., 2013) global-coverage aerosol products (de Leeuw et al., 2015; Popp et al., 2016) are selected, including the AATSR-ADV, AATSR-SU, AATSR-ORAC and AATSR-ENSEMBLE. The AATSR-ADV product is generated using the dual view (ADV) and single view (ASV) algorithms over the land and oceans (Veefkind and de Leeuw, 1998), respectively. The ADV algorithm uses the dual view feature and the k-ratio approach (Flowerdew and

105 Haigh, 1995) to eliminate the surface contribution to the apparent reflectance. First, the aerosol contribution at 1.61 μm is assumed to be negligible, and then, the aerosol contribution is given a value during continuous iteration steps. However, this approximation is not reliable over bright surfaces or in the presence of coarse mode aerosols. The ASV algorithm assumes the water is a dark surface at the near-infrared channel, and an ocean reflectance model is applied to correct for the effects of chlorophyll and whitecaps (Kolmonen et al., 2016). The SU algorithm employs a parameterized model of the surface angular

110 anisotropy and estimates the surface spectral reflectance using the dual view feature over land. Over the ocean, the SU algorithm estimates the low ocean leaving radiance at the red and infrared channels at both nadir and along-track view angles with a simple model (North et al., 1999; North, 2002). The ORAC algorithm is an optimal estimation retrieval scheme for multispectral images (Poulsen et al., 2012; Sayer et al., 2011; Thomas et al., 2009). The ORAC algorithm uses a forward model to fit all the shortwave forward and nadir radiances through the DIScrete Ordinate Radiative Transfer (DISORT)

115 model. Meanwhile, the retrieved errors for aerosol parameters are estimated by propagating the measurement and forward model uncertainties into the state space. The AATSR-ENSEMBLE (AATSR-EN) product is integrated based on different ESA-AATSR aerosol products using likelihood estimate approaches (Holzerpopp et al., 2013). In this study, the latest versions of the above four ESA-CCI products (Table 1) are collected from the ICARE Data and Services Centre (http://www.icare.univ-lille1.fr/cci).

120

2.1.2 AVHRR aerosol product

The AVHRR aerosol product is only available over the oceans and is generated based on the two-channel aerosol retrieval algorithm (Stowe et al., 1997; Ignatov and Stowe, 2000). AVHRR assumes that the molecular atmosphere, aerosol microphysics, and surface reflectance are known, and based on the radiative transfer model, the aerosol retrieval is

125 performed independently at the visible (0.63 μm) and near-infrared (0.83 μm) channels through the precalculated LUT (look-up table). A bimodal lognormal aerosol size distribution is selected to represent the fine and coarse modes. Meanwhile, gaseous absorption, aerosol scattering, and polarization effects are further corrected (Zhao et al., 2004).

2.1.3 MISR aerosol product

130   The MISR aerosol product provides aerosol distributions over both land and oceans. Over land, MISR is initially based on
the dense dark vegetation (DDV) algorithm (Kaufman and Sendra, 1988, King et al., 1992) and uses spatial contrasts to
explore an empirical orthogonal function of the angular variations of apparent reflectance. Then, MISR is used to estimate
the scene path radiance and determine the best-fitting aerosol models. In addition, the spectral and angular shapes of the
reflectance function are assumed to be constant. Over the ocean, the water bodies are essentially assumed to be black at

135   visible and near-infrared wavelengths, and with an additional assumption of an ocean aerosol model, the aerosol retrieval is
realized using the radiative transfer (RT) theory. Multi-angle radiances from MISR, which are strongly affected by the
aerosol scattering phase functions, help to improve the definition of aerosol models used in aerosol retrieval (Martonchik &
Diner, 1992; Martonchik, 1997; Martonchik et al., 1998). In this study, the newest version 23 (V23) of MISR aerosol
retrievals over land and ocean (Kalashnikova et al., 2013; Martonchik et al., 2009) are obtained for use from the NASA

140   Langley Atmospheric Sciences Data Center (https://eosweb.larc.nasa.gov/project/misr/misr_table).

2.1.4 MODIS aerosol products

The MODIS aerosol products are generated from three well-known algorithms, including the dark target (DT) algorithms
over both the oceans and land and the deep blue (DB) algorithm over only land. Over the oceans, the DT algorithm considers

145   the water as a dark surface from visible to longer wavelengths and neglects the water surface reflectance. Over land, the DT
algorithm assumes that the surface reflectances in the visible channels are in stable statistical empirical relationships with the
2.1 μm apparent reflectance over the dark target surfaces (Kaufman et al., 1997; Levy et al., 2007). The aerosol retrieval can
be realized based on the atmospheric RT model using the LUT approach. In contrast, the DB algorithm is designed to
overcome the flaw in DT and realizes aerosol retrieval over bright surfaces, where the surface reflectance for visible

150   channels is estimated based on the precalculated surface reflectance database using the SeaWiFS surface reflectance products
(Hsu et al., 2004, 2006). Later, the two algorithms were continuously improved, and the second-generation operational DT
(Levy et al., 2013) and the enhanced DB algorithms (Hsu et al., 2013) were used to generate the latest operational aerosol
products. Recently, to increase the data coverage, a DT and DB (DTB) combined dataset was generated according to the
independently derived MODIS monthly normalized difference vegetation index (NDVI) products that leverage the strengths

155   of the DT and DB algorithms (Levy et al., 2013). Therefore, in this study, the most recently released Terra and Aqua
Collection 6.1 (C6.1) Level 3 combined DT and DB aerosol products are selected.

2.1.5 SeaWiFS aerosol product

The SeaWiFS aerosol product over land is generated from the same DB algorithm as MODIS (Hsu et al., 2004, 2006). Over

160   the ocean, the SeaWiFS aerosol product is based on the SeaWiFS Ocean Aerosol Retrieval (SOAR) algorithm (Sayer et al.,
2012) and includes three phases: a preprocessing step for cloud screening, aerosol retrieval, and a postprocessing stage (data
downscaling and quality assurance). In SOAR, the aerosol retrieval simultaneously determines the AOD and fine mode
volume fraction using a forward model (FM) based on the linear interpolation of precalculated LUTs. In addition, for aerosol

microphysical models, a bimodal lognormal distribution is used to assume that the aerosol particles are in the pure maritime
165   mode and pollution and dust-influenced modes.

2.2 AERONET ground measurements

Aerosol Robotic Network (AERONET) ground-based measurements are collected to validate the above nine operational
global aerosol products in this study. AERONET is a widely used ground-based observation network with long-term data
170   records at numerous monitoring sites around the world. The AOD observations are available in a wide spectral range from
visible to near-infrared channels (0.34–1.02 μm) at a high temporal resolution of 15 min and a low bias of 0.01–0.02. The
observations are divided into three levels (L): L1.0 (unscreened), L1.5 (cloud screened), and L2.0 (cloud screened and
quality assured) (Holben et al., 1998). In the current study, the latest released AERONET Version 3 L2.0 monthly AOD
observations at a total of 210 sites over land and 33 sites over the oceans are collected with a criterion that each site has at
175   least 2 years (24 monthly) of observations. The globe is divided into eight custom regions of land, five coastal areas and
three open ocean areas, as illustrated in Figure 1.

3 Methodology

3.1 Spatial comparison

For multisatellite aerosol products, only the monthly retrievals (averaged from the daily mean values) at 550 nm with
180   sufficiently high-quality assurance obtained from the listed scientific dataset (SDS, Table 1) are selected for the current
analysis. Due to different spatial resolutions, all datasets are uniformly integrated into a 1°× 1° grid cell using the bi-
directional linear interpolation method. For comparison, monthly retrievals for diverse aerosol products are defined by the
pixel centred on the AERONET site, and the corresponding monthly AERONET AOD is the true value. To explore the
spatial distributions and temporal trends of aerosol loadings, the annual mean values for each dataset are averaged pixel by
185   pixel from at least eight available monthly retrievals over one year. Notably, the AERONET sites do not provide the AOD
observations at 550 nm; therefore, AOD values at 550 nm are interpolated using the Ångström exponent (α) algorithm in the
440–675 nm wavelengths using AERONET AODs measured in those wavelengths (Eq. 1) (Sun et al., 2016; Wei & Sun,
2017; Wei et al., 2017; 2018). Table 1 summarizes the data sources used in this study.

$$AOD_{550} = AOD_{\lambda}(550/\lambda)^{-\alpha} \ (1)$$

190   **3.2 Temporal trend**

Linear trends were calculated based on the monthly mean aerosol datasets. An additional criterion for the monthly AOD
trends is at least five years (120 monthly values) of observations for each selected AERONET site. If this condition is not

met, monthly trends are not calculated and not included in the trend analysis. To remove the effects of the seasonal

variations, the data were first deseasonalized by calculating the AOD anomaly for each grid cell. The anomaly is defined as

195 the difference between monthly retrievals and the month-wise average over all the years. Then, the least squares fitting

method is applied to the monthly anomaly AODs to obtain the slope coefficient of the linear regression that represents the

annual trend (AOD yr^{-1}, Eq. 2). A bilateral T-test is used to assess the statistical significance of the calculated trends. To

quantify the correctness of each satellite aerosol product in capturing aerosol trends, a correct-trend percentage (CTP) is

calculated as a percentage of sites showing the same trend symbols from the satellite product and from the AERONET

200 measurement (Eq. 3).

$$Y_t = aX_t + b + N_t, t = 1, …, T \text{ (2)}$$

$$CTP = \frac{N_c}{N_{all}} * 100 \text{ (3)}$$

where Y_t is the anomaly AOD time series, a is the trend (AOD yr^{-1}), b is the offset term, and X_t is the annual time series (X_t

= t/12, where t is the individual month in the time series). The term N_t represents the noise in the time series. N_c represents

205 the number of sites showing the same trend symbols from the satellite product and from the AERONET measurement, and

N_{all} represents the number of all the available sites for analysis.

3.3 Statistical metrics

To quantitatively evaluate the quality and uncertainty of the retrievals, several metrics are calculated between the AOD

retrievals (AOD$_{Retrieval}$) and AERONET AOD measurements (AOD$_{AERONET}$), including the Pearson product-moment

210 correlation coefficient (R), mean absolute error (MAE, Eq. 4), mean bias (MB, Eq. 5), root mean square error (RMSE, Eq.

6), relative mean bias (RMB, Eq. 7), and MODIS expected error (EE, Eq. 8, Levy et al., 2013) envelope:

$$MAE = \frac{1}{n}\sum_{i=1}^{n}|AOD_{Retrieval} - AOD_{AERONET}| \text{ (4)}$$

$$MB = \frac{1}{n}\sum_{i=1}^{n}(AOD_{Retrieval} - AOD_{AERONET}) \text{ (5)}$$

$$RMSE = \sqrt{\frac{1}{n}\sum_{i=1}^{n}(AOD_{Retrieval} - AOD_{AERONET})^2} \text{ (6)}$$

215 $$RMB = \frac{1}{n}\sum_{i=1}^{n}|AOD_{Retrieval}/AOD_{AERONET}| \text{ (7)}$$

$$EE = \pm(0.05 + 0.2 * AOD_{AERONET}) \text{ (8)}$$

4 Statistical validation of aerosol products

4.1 Performance at the global-scale

First, we validate the operational aerosol products against the AERONET AOD measurements at the global-scale and in the

220 available periods of the products. Figure 2 compares the monthly AODs in eight land regions. Four ESA-CCI AATSR

aerosol products show similar performances with small relative differences within 5% for the main evaluation metrics (e.g.,

fractions within EE, MAE, and RMSE). MISR and MOD08 are both aboard the Terra platform, and these products perform almost equally with similar data collections and fractions within the EE, MAE, and RMSE values. The MYD08 product performs well, with a high percentage of collections falling within the EE (~77%) and small MAE and RMSE values of

225   0.067 and 0.109, respectively. The SeaWiFS product provides minimum data collection due to having the shortest operational period among all products. Approximately 74% of the SeaWiFS retrievals fall within the EE with an average MAE of 0.077 and RMSE of 0.125. In general, all aerosol products agree well with the ground observations, with at least 70% of the retrievals meeting the requirements of the EE and with adequate MAE (0.06-0.09) and RMSE (0.11-0.15) values over land.

230   For statistical comparison, we extract and validate the retrievals against AERONET AODs in their common period (2003-2010) over land (Table 2). Due to the differences in aerosol retrieval algorithms, the space coverage is not uniform among these eight products, resulting in noticeable differences in the number of data collections. MISR provides the maximum data collection. SeaWiFS has the minimum coverage over land, with data collection numbers that are 37% less than MISR. MYD08 showed the best performance, with the highest fraction (~75%) within EE and the lowest MAE (~0.065) and RMSE

235   (~0.104) values. AATSR-ADV has relatively worse evaluation metrics than all other products.
Similar validations over eight ocean areas are plotted in Figure 3. A smaller number of retrievals is collected over the oceans than land due to sparse ground observation sites, and the monthly aerosol concentrations are generally below 0.4. For the four ESA-CCI AATSR aerosol products, the SU algorithm performs the best, with approximately 80% of the monthly retrievals matching the acquirements of EE and with the lowest MAE and RSME values. The EN algorithm is better than

240   both the ORAC and ADV algorithms. AVHRR, MISR and MODIS provide larger and similar numbers of data collections due to their longer observational periods. The three products MYD08, MISR and AVHRR show good performances, with more than 74% of the retrievals falling within the EE and small MAE and RMSE values of 0.06 and 0.07, respectively. SeaWiFS has the least data collection similarity to the over-land statistics. However, the performance of SeaWiFS over the ocean is improved, with 82% falling within the EE and with relatively low estimation uncertainty (MAE=0.049,

245   RMSE=0.071). In general, all aerosol products agree well with the ground observations, with at least 66% of the retrievals falling within the EE and with considerably low MAE (0.04-0.07) and RMSE (0.06-0.10) values over all the ocean areas. Statistical comparisons of nine AOD retrievals with AERONET AOD over the ocean are also indicated in Table 2 in the common period (2003-2010). MODIS products have the largest number of successful retrievals, while SeaWiFS has the least successful retrievals over the ocean. Among all nine products, MYD08 shows the best performance with good evaluation

250   metrics (MAE=0.05, RMSE=0.067 and fraction falling within EE= 78.29%), while the AATSR-ORAC algorithm shows the worst performance with the largest estimation uncertainty. Notably, Terra MODIS has a larger estimation uncertainty and thus a noticeably lower accuracy than Aqua MODIS over the ocean.

4.2 Performance at the site scale

The global-scale validation in Section 4.1.1 evaluates the overall performance of the nine different aerosol products.
255 However, the selected AERONET sites are unevenly distributed around the world, with most sites concentrated in the densely populated land regions. Therefore, site-level validation is performed in this section to further evaluate the nine products. For this purpose, three main evaluation metrics are calculated, including correlation (R, reflects the temporal consistency between monthly retrievals and measurements), a fraction of the retrieval matching in the EE (*f*, reflects the overall performance) and MB (reflects the over/underestimation uncertainty). For statistical significance, only those sites
260 with at least 2 years of observations (24 matchups) are used for analysis.

Figure 4 illustrates the distribution of retrieval percentages falling within the EE at each site. Good performances (*f* > 80%) are mostly seen in the North American and European sites. However, all algorithms show poor performances in Africa and Asia, with less than 40% of the retrievals meeting the accuracy requirement. In general, MYD08 has the best performance at the site scale, with high fractions matching the EE (*f* > 60%) at ~83% of the 242 selected sites, while MOD08 has the worst
265 performance, with only 66% of the sites showing good matching (*f* > 60%) among all aerosol products. In addition, 72%, 74%, 68%, 77%, 74% and 76% of the sites show good matching (*f* > 60%) for four RSA-CCI AATSR (ADV, EN, ORAC, and SU), MISR and SeaWiFS aerosol products, respectively. Finally, 82% of the 34 AVHRR product ocean sites match well.

Figure 5 plots the correlations between retrievals from each satellite product and AERONET measurements for all available
270 sites. Good consistencies are mainly distributed in sites over North America, southern Europe, and central South America, while poor consistencies are observed in Asia, southern South America, and the ocean sites. AVHRR monthly retrievals agree well with ground measurements (R>0.6) at 58% of the ocean sites, especially for those sites close to the mainland. MISR and SeaWiFS products have high consistencies (R>0.6) for 55% and 52% of the sites, respectively. The four ESA-CCI products perform similarly to the MISR and SeaWiFS but have fewer sites with correlations greater than 0.6. For
275 MODIS products, much "deeper" colours are always seen at most sites around the world compared to the other aerosol products, indicating the superior agreement of MODIS products with the ground measurements. Approximately 76% and 81% of the sites show high consistencies (R>0.6) for the MOD08 and MYD08 products, respectively.

Figure 6 depicts the MB of retrieved AOD to AERONET AOD for each of the nine products. Both AATSR-EN and ORAC aerosol products have equally good estimations, with ~35% of the sites having a low mean absolute bias (<0.02).
280 Overestimations are frequently observed in most North American and European sites, while those sites in South America, Africa, and Asia show considerable underestimations. AVHRR underestimates at the sites along the coast of Europe. SeaWiFS, ATSR-ADV and MISR strongly underestimate at ~80%, ~61% and ~60% of the sites, respectively. In contrast, MOD08 and MYD08 have obvious overestimations at ~83% and ~75% of the sites, respectively. In general, ATSR-SU shows the smallest estimation uncertainty at more than half (~51%) of the sites with a mean absolute bias of less than 0.02.

5 AOD spatial distributions

5.1 Global AOD distribution

In this section, we compare the overall global aerosol distributions among the nine products by focusing on their similarities and differences. The eight common-year (2003-2010) averaged AOD are shown in Figure 7. All aerosol products capture the first-order spatial patterns that high aerosol loadings (AOD>0.6) are mostly in mainland regions, including Africa, the Middle East, India, and East Asia and the corresponding coastal areas. In contrast, the annual mean AODs are generally less than 0.3 in the rest of the continental and ocean areas.

Figure 7 shows the different spatial coverages among the nine products, which is apparently due to the principle and ability of the respective aerosol algorithms of each product. All aerosol products can provide full spatial coverage distributions over the ocean due to homogeneous surfaces and low surface reflectance characteristics. However, aerosol retrieval over land becomes more challenging with complex surface structures (Wei et al., 2017). The SeaWiFS product shows the poorest spatial continuity with numerous missing values in northern South America and central and northern Asia. The AATSR-ADV algorithm fails to generate aerosols in northern Africa, the Middle East or Central Asia due to the algorithms' limitations in bright desert areas. The remaining six algorithms can provide nearly full spatial coverage over land except for permanent snow/ice areas in high-latitude and high-altitude areas.

5.2 Regional AOD distribution

Despite the overall similarity in global AOD spatial distributions, noticeable numerical differences still exist in local regions and require quantitative comparison. For this purpose, we obtain the mean AOD over the eight land regions and eight oceanic regions. Figure 8 shows the regional AOD values over the land, ocean and in each of the custom regions among different aerosol products from 2003-2010. The eight-year mean AOD is 0.18±0.03 over land (Figure 8a). Among all the datasets, SeaWiFS shows the lowest annual AOD values over most land regions, followed by the MISR product. Conversely, AATSR-SU and Terra MODIS show the highest annual mean AODs over most land regions. In general, noticeable differences are found in most regions with absolute AOD differences greater than 0.1. Especially in North Africa (NAF), Central Africa (CAF), the Middle East (ME), and East Asia (EAA), these large differences exceed 0.2. Notably, AATSR-ADV exhibits the lowest annual mean AOD in NAF and the ME with a large number of missing values in both regions due to the limitation of the AATSR-ADV algorithm.

There are relatively small differences in the annual mean AOD values among all satellite products over the oceans (Figure 8b) than over land. The eight-year mean oceanic AOD is 0.13±0.02. Similar to the features over land, SeaWiFS frequently has the lowest annual AOD values, while AATSR-ADV and MOD08 have annual AOD values that are higher than the other products. In the three open ocean areas (Pacific Ocean (PAOC), Atlantic Ocean (ATOC), and INOC), the differences among datasets are less than 0.08. However, in the five offshore areas close to the land aerosol sources, larger differences can be

observed. Especially in the coastal areas of western North America (CWNA), south Asia (CSAA) and East Asia (CEAA), the annual mean AOD differences exceed 0.11.

To further explore the accuracy in regional AODs among different products, we calculate the MB between the satellite-derived and AERONET-measured annual mean AODs from 2003 to 2010. Figure 9 shows the mean AOD bias for all nine

320 aerosol products as a function of the year over 7 land regions and over the oceans. The land region of CAF and the 8 oceanic regions are not plotted because of a lack of AERONET data. The statistics of the mean AOD bias among the nine aerosol datasets are shown in Table 3.

Figure 9 and Table 2 indicate positive mean biases in four of the ESA-CCI AATSR and MODIS aerosol products, while MISR (~-0.007) and SeaWiFS (~-0.013) show slightly negative mean biases. In northern South America (NSAM), the biases

325 of eight land products show strong variations over the past decade. All land products except MISR and AATSR-ORAC show positive biases in most years in NSAM (note that we did not obtain the SeaWiFS biases due to the frequent absence of data in this region). In Europe (EUR), the MOD08 (~0.038) and MYD08 (~0.015) products have positive biases, and all other products show stable negative biases, suggesting overall underestimations. Similar conclusions are obtained for South Asia (SAA) and EAA but with stronger variations. NAF has negative and largely varying biases in most years, where the MODIS

330 biases recently became positive and close to zero. In the ME, AATSR-ADV (~-0.051), ORAC (~-0.021) and SeaWiFS (~-0.03) have negative biases, and all the other products show large positive biases, suggesting serious overestimations. In the overall land area, bias variations in different custom regions cancel each other out and result in nearly uniform biases for all aerosol products. The MOD08 (~0.035) and MYD08 (~0.019) products always overestimate the land AOD, while most of the others underestimate the land AOD. AATSR-SU (~0.009) appears to be the most accurate with the smallest biases in the

335 land AOD.

Over the oceans (Figure 9i), AVHRR (~-0.031) underestimates the aerosol loadings with large negative biases over time. The SeaWiFS, AATSR-EN, and AATSR-SU products show similar underestimations before 2005 and recently shifted to overestimations. In contrast, AATSR-ADV (~0.03), AATSR-ORAC (~0.044), MOD08 (~0.054), MYD08 (~0.035) and MISR (~0.018) show stable positive biases over time, indicating overall overestimations.

340 **5.3 AOD distribution validation at the site scale**

Figure 10 compares the annual mean AOD retrievals to the AERONET measurements at all available sites for nine operational aerosol products over the land and oceans. For this purpose, AERONET sites with at least two years (24 months) of effective ground observations are used. The red dots in Figure 10 are over-land areas. Among the four ESA-CCI AATSR products, the SU algorithm shows the best performance, with the lowest MAE (~0.041) and RMSE (~0.063) values and a

345 small overestimation uncertainty (RMB=1.009). The EN algorithm shows the next best performance. The other two AATSR products show approximately 11% underestimation uncertainties with larger MAE and RMSE values. The annual mean MISR retrievals are generally lower than the ground observations at most sites, with an underestimation uncertainty of 16%. The MAE and RMSE values are 0.055 and 0.091, respectively. SeaWiFS also shows a large underestimation uncertainty

(MAE=0.048, RMSE = 0.078, and RMB=0.823). The MODIS products have noticeably high correlations with ground

350   measurements (R>0.931). MOD08 shows an ~20% overestimation uncertainty (RMB=1.204) with MAE and RMSE values
of 0.056 and 0.070, respectively. MYD08 shows an overall better performance compared to the MOD08 product, suggesting
more accurate estimations in the annual mean aerosols over land. In summary, the AATSR-SU and MYD08 products capture
the annual mean AOD over land with the best accuracy.

The blue dots in Figure 10 show validations over the ocean. Among the four ESA-CCI AATSR products, the SU algorithm

355   provides the most accurate annual mean AOD with the lowest MAE, RMSE and RMB values, which is followed by the EN
algorithm. The other two AATSR products show serious overestimation uncertainties with large MAE and RMSE values.
The MISR product shows a similar performance to AATSR-ORAC. MODIS again shows the highest correlations with the
ground measurements among all oceanic products. However, MOD08 has a poor performance, while MYD08 performs
much better. AVHRR strongly underestimates (RMB=0.88) the annual mean AOD, which is the opposite of the other

360   oceanic products. In summary, the AATSR-SU and EN products capture the annual mean AOD over the ocean with the best
accuracy.

6 AOD temporal trends

6.1 Global aerosol trends

In this section, we focus on the temporal trends of global and regional AOD products. Similar to Section 5, the spatial

365   distributions and differences in aerosol trends during 2003-2010 among all the satellite datasets are calculated. The aerosol
trends are derived from the monthly retrievals (at least 60 monthly values are available) for each product using the least
squares fitting method, as mentioned in Section 3.2.

The global AOD trend distribution (Figure 11) shows similar overall spatial patterns among all aerosol products. Over land,
the significantly increasing trends (a>0.01, p<0.01) are mainly found in the ME and SAA, indicating an elevated level of air

370   pollution over the past two decades. In contrast, negative aerosol trends (a>0.01, p<0.01) are observed in eastern North
America, Europe, CAF, and EAA, indicating improved air quality. Over the oceanic areas, the spatial differences in aerosol
trends are relatively smaller than those observed over land. Decreasing AOD trends mainly occur in coastal areas of eastern
North America, western NAF, and EAA. Increasing aerosol trends occur in most of the remaining oceanic areas. Notably,
the coastal areas of SAA have the strongest AOD trends over the oceans. However, aerosol heterogeneity trends still exist

375   among diverse products. Four ESA-CCI AATSR and MISR products show similar spatial patterns, whereas the MOD08,
MYD08, and SeaWiFS products are consistent in most areas. An outlier is AVHRR, which shows significantly increasing
aerosol trends in most oceanic regions (p<0.05). Readers may also notice that the four ESA-CCI AATSR and MISR products
are quite noisy, while the remaining products show smoother distributions, which might be attributed to the spatial coverage
of the data and the treatment of retrievals in neighbouring pixels.

6.2 Regional AOD trends

Despite the similar spatial distributions in global AOD trends, variations in aerosol trends among all the satellite products are apparent in local regions. Therefore, the aerosol trends during the common period (2003-2010) for the custom land and oceanic regions are investigated in Figure 12. Over the land areas, the AATSR-SU, MISR, and MYD08 products show the same increasing trends, while the other products show decreasing trends in aerosols (Figure 12a). In the eight land regions, most satellite products in both the ME and SAA have significantly large positive trends ($p<0.05$), while the other six regions have decreasing aerosol trends. However, noticeable variations in AOD trends (absolute trend differences greater than 0.005 per year) still exist in NAF, the ME, and SAA.

Similar conclusions can be obtained for the AOD trends over the ocean, where all aerosol products show nearly the same sign of trends but with certain variations in individual regions (Figure 12b). Over the global ocean and three open ocean areas (PAOC, ATOC, and the Indian Ocean (INOC)), AVHRR always shows the most strongly and significantly increasing trends ($a>0.002$ and $p<0.02$) among all aerosol products. In contrast, the aerosol trends observed by AVHRR in most coastal regions (CENA and CWNA, CEUR, and CSAA) are closer to 0 and distinctly different from the other products. Moreover, large variations in aerosol trends greater than 0.004 per year are observed in CWSA, CSAA and CEAA.

6.3 AOD trend validations at the site scale

To quantitatively evaluate the accuracy of AOD trends from different aerosol products, the satellite-derived aerosol trends are validated against those calculated from AERONET ground measurements. To ensure the statistical significance of the trend calculations, only the AERONET sites with at least 5 years (120 months) of effective observations are selected for validation purposes. Then, the AOD trends from multiple satellite products and AERONET data are calculated for each site using the same simple line regression approach (see Section 3.2).

Red dots indicate validations over land in Figure 13. The AATSR-ADV, AATSR-EN, AATSR-ORAC and AATSR-SU products have 77%, 77%, 75% and 82% of sites, respectively, showing the same trend sign as the trend from AERONET. The four ESA-CCI AATSR products perform similarly in describing the aerosol temporal variations. MISR shows an overall better performance than the four AATSR products over land. MOD08 captures the most accurate aerosol trends (81% of sites with the same sign as the AERONET-measured trend) with the lowest MAE and RMSE values of 0.027 and 0.038, respectively. MYD08 performs almost equally to MOD08. SeaWiFS shows a similar performance to the AATSR-ADV product with nearly the same evaluation metrics. In summary, the MISR and MODIS products capture the aerosol temporal variations over land most accurately among all datasets.

Blue dots show the validations over the ocean in Figure 13. Far fewer sites can be collected over the ocean than over land due to the lack of AERONET stations and short observation times. For the four ESA-CCI AATSR products, the ADV algorithm has the best performance, with 88% of the sites showing trends that are consistent with ground measurements and with the lowest MAE value of 0.033. The SU and EN algorithms show the next best performances. The ORAC algorithm

performs the worst with the largest MAE and RMSE values and with only 67% of the sites capturing the correct AOD trends. MISR provides more accurate AOD trends than most of the ESA-CCI products. MOD08 and MYD08 have similar good performances, with 90% and 84% of the sites, respectively, having the same sign of AOD trends as AERONET.

415 AVHRR performs similarly with AATSR-SU but generally worse than the MISR and MODIS products. In summary, the two MODIS products are the most accurate in capturing the aerosol trends over the oceans among all datasets.

6.4 Aerosol trends over the past two decades

Based on the above analysis of the monthly and annual data, we conclude that MODIS products capture AOD trends with the best accuracy among the nine operational global aerosol products, although the MODIS products tend to overestimate the

420 aerosol loadings. Therefore, we take the Terra MODIS product (Terra has longer records than Aqua) as a representative to study aerosol evolution over the past two decades. Figure 14 shows aerosol trends over both land and oceans derived from MOD08 monthly AODs at 550 nm for each 1°× 1° grid cell from January 2000 to December 2017. Overlain black dots indicate regions with trends significant at the 95% confidence level. Notably, the aerosol trends are not available at higher latitudes than 50°N/S due to a large number of missing values in winter.

425 The MOD08-derived AOD trends are generally weak (a<0.0025 per year) across most of the globe. The average AOD trend over the entire land area is -0.0001 yr^{-1} and is not statistically significant. However, trends in some specific land regions are worth noting. For example, fast-developing countries such as India in SAA and north China in EAA show significantly increasing aerosol trends (regional average a>0.0027 yr^{-1} and $p<0.05$). In the dust dominant regions, such as the Arabian Peninsula and Central Asia, positive trends (average a>0.017 yr^{-1} and $p<0.05$) are also observed, and the increasing trends in

430 the western United States and CAF can possibly be attributed to the biomass burning of forest fires. In contrast, significantly negative trends are found over the eastern US (-0.0027 yr^{-1}, $p<0.05$), EAA (-0.0025 yr^{-1}, $p<0.05$, especially in central and southern China and Japan) and Europe (-0.0022 yr^{-1}, $p<0.05$). Decreasing trends are also seen over vast biomass burning regions, such as central South America and the western Savanna in Africa but are not statistically significant.

The global ocean shows a strong average positive trend of 0.0005 yr^{-1}, which meets the statistical significance of the 95%

435 confidence level and indicates significant but weak increasing trends over most marine areas. On the regional scale, the PAOC (a=0.0008 yr^{-1} and $p<0.05$), ATOC (a=0.0014 yr^{-1} and $p<0.05$), and Indian Ocean (a=0.007 yr^{-1} and $p<0.05$) have strong positive trends. Moreover, significantly increasing trends are also observed in coastal areas of the SAA (0.0035 yr-1, $p<0.05$). In contrast, significantly negative trends are found over the coastal areas of Europe (-0.0017 yr^{-1}, $p<0.05$), the eastern US (-0.0016 yr^{-1}, $p<0.05$) and western South America (-0.007 yr^{-1}, $p<0.05$). Downward trends observed in western

440 Africa and eastern Asia are not statistically significant.

To further explore the interannual aerosol variations in different regions, the time series of annual mean MOD08 AOD from 2000 to 2017 for eight land and eight ocean regions are calculated and shown in Figure 15. Over land, both Europe and Eastern North America show significant and continuous trends of aerosol reduction ($p<0.05$) over the past 20 years, which is

partly because of the decrease in pollution aerosols associated with emission control. NSAM also has a continuously

445   decreasing trend with interannual fluctuations; thus, the trend is not statistically significant. Air pollution is significantly and continuously increasing ($p<0.05$) over SAA, and the air pollution trend is mainly related to an acceleration of urbanization or industrialization. Interestingly, the aerosol trend observed in EAA shifted from a strong positive trend before 2008 to a significant negative trend ($p<0.05$) after 2010, which is similarly to the result reported in (de Leeuw et al., 2018). This shift likely occurred because of the Chinese government's policy aiming to reduce pollutant emissions, which was proposed and

450   applied in approximately 2010. The ME shows a significantly increased trend before 2010 due to frequent dust storms, as a previous study reported (Hsu et al., 2012), but recently shifted to a decreasing trend. NAF exhibits a relatively stable trend before 2009 and recently changed to a decreasing trend. Over the entire global land area, the interannual aerosol variation is weak.

Figure 15b shows the results over the oceans. The coastal areas of eastern North America, Europe, and western South

455   America show continuously decreasing trends ($p<0.05$) during the entire period. In contrast, continuously increasing trends ($p<0.05$) are found in the Pacific, Atlantic and Indian Oceans. The coastal area of SAA shows a flat trend in the first few years changing to a significantly increasing trend after 2005, which is very likely related to both the dust transport from the ME and enhanced human activities. The coastal area of EAA has a strongly increasing trend before 2005 and subsequently shifted to a significantly decreasing trend ($p<0.01$). The downward trend in CEAA is mostly affected by the reduction of

460   pollutant emissions in the continental source regions. Over all global oceans, a continuously increasing aerosol trend ($p<0.05$) is observed (dark curve in Figure 15b). In general, aerosol variations are relatively weak in most marine areas, mainly due to the lesser effects of human activities, especially in the open ocean areas.

7 Summary and conclusion

The focus of this study is on the similarities and differences in spatial variations and temporal trends of the currently

465   operational satellite-derived aerosol optical depth products. For this purpose, nine global aerosol products are collected and validated against the AERONET ground measurements from 243 AERONET sites over the land and oceans, including four products from the European Space Agency's Climate Change Initiative (AATSR-ADV, AATSR-EN, AATSR-ORAC, and AATSR-SU), and the AVHRR, MISR, SeaWiFS, Terra and Aqua MODIS products. Validations and comparisons are performed in three ways: 1) statistical validation of monthly AOD retrievals against AERONET measurements on global and

470   site scales; 2) AOD spatial distributions on global, regional and site scales; and 3) AOD temporal trends on global, regional and site scales.

Our results show that noticeable differences are observed in the spatial coverage and aerosol spatial distributions among the nine products. SeaWiFS and AATSR-ADV products have poor spatial continuities with numerous missing values, while the other products can provide nearly full spatial coverages. Large differences in AOD values are found in NAF, CAF, the ME,

475   and EAA, as well as in the CWSA, SAA and EAA. In general, the AATSR-SU algorithm describes the aerosol distributions

most accurately over both the land and oceans. The MISR and SeaWiFS products seriously underestimate, yet MODIS products strongly overestimate the annual mean aerosols over land. All the products overestimate the AOD over the ocean except AVHRR.

In terms of temporal trends, most of the products behave similarly with a decreasing trend over the ocean, but AVHRR
480   shows the opposite trend. Differences in the trend magnitudes are found in open oceans and in the coastal areas of western South America, Southeast Asia and EAA. More than 75% of the sites capture the correct sign of aerosol trends over land, although numerical inconsistencies occur mostly in NAF, the ME, and SAA. In general, MODIS products appropriately reproduce the aerosol trends over the land and oceans among all datasets.

Finally, we analyse the aerosol trends over the past two decades by using the Terra MODIS product as a representative. Air
485   pollution is continuously increasing (p<0.05) in SAA, mainly related to accelerated urbanization and industrialization. However, the AOD trend in EAA shows increasing air pollution in the first decade and subsequently shifts to the opposite trend, mainly due to the greatly reduced pollutant emissions. However, the reasons for the change in aerosol trends in specific regions need to be further explored. This study quantifies the performance of multiple aerosol products and evaluates the abilities of these products in describing the spatial distribution and temporal trends of aerosols. Our results may
490   help readers to better understand the features of different satellite aerosol products and to choose a suitable aerosol dataset for their respective research studies.

Acknowledgements

The ESA-CCI AATSR and AVHRR monthly products are obtained from the ICARE Data and Services Centre (http://www.icare.univ-lille1.fr/cci). The MODIS and SeaWiFS monthly products are available at
495   https://search.earthdata.nasa.gov/, and the AERONET measurements are available from the NASA Godard Space Flight Center (https://aeronet.gsfc.nasa.gov/). This work was supported by the National Natural Science Foundation of China (71690243, 41775137 and 41761144056) and National Important Project of the Ministry of Science and Technology in China (2017YFC1501404). All authors made substantial contributions to this work. Y. Peng designed the research, and J. Wei carried out the research and wrote the initial draft of this manuscript. R. Mahmood, L. Sun and J. Guo helped review the
500   manuscript. We declare no conflicts of interest.

References

Bartell, S. M., Longhurst, J., Tjoa, T., Sioutas, C., & Delfino, R. J. (2013). Particulate air pollution, ambulatory heart rate variability, and cardiac arrhythmia in retirement community residents with coronary artery disease. Environmental Health Perspectives, 121(10), 1135.

505   Brauer, M., Amann, M., Burnett, R. T., Cohen, A., Dentener, F., & Ezzati, M., et al. (2012). Exposure assessment for estimation of the global burden of disease attributable to outdoor air pollution. Environmental Science & Technology, 46(2), 652-660.

Cao, J. J., Wang, Q. Y., Chow, J. C., Watson, J. G., Tie, X. X., & Shen, Z. X., et al. (2012). Impacts of aerosol compositions on visibility impairment in Xi'an, China. Atmospheric Environment, 59, 559-566.

510   Crouse, D.L., Peters, P.A., van Donkelaar, A., Goldberg, M.S., Villeneuve, P.J., Brion, O., et al., 2012. Risk of nonaccidental and cardiovascular mortality in relation to long-term exposure to low concentrations of fine particulate matter: a Canadian national-level cohort study. Environ. Health Perspect. 120 (5), 708–714.

de Leeuw, G., T. Holzer-Popp, S. Bevan, W. Davies, J. Descloitres, R.G. Grainger, J. Griesfeller, A. Heckel, S. Kinne, L. Klüser, P. Kolmonen, P. Litvinov, D. Martynenko, P.J.R. North, B. Ovigneur, N. Pascal, C. Poulsen, D. Ramon, M.
515   Schulz, R.Siddans, L. Sogacheva, D. Tanré, G.E. Thomas, T.H. Virtanen, W. von Hoyningen Huene, M.Vountas, S. Pinnock (2015). Evaluation of seven European aerosol optical depth retrieval algorithms for climate analysis, Remote Sensing of Environment, 162, 295–315.

de Leeuw, G., Sogacheva, L., Rodriguez, E., Kourtidis, K., Georgoulias, A. K., Alexandri, G., Amiridis, V., Proestakis, E., Marinou, E., Xue, Y., and van der A, R. (2018): Two decades of satellite observations of AOD over mainland China
520   using ATSR-2, AATSR and MODIS/Terra: data set evaluation and large-scale patterns, Atmospheric Chemistry & Physics, 18, 1573-1592.

Flowerdew, R. J., & Haigh, J. D. (2013). An approximation to improve accuracy in the derivation of surface reflectances from multi-look satellite radiometers. Geophysical Research Letters, 22(13), 1693-1696.

Fraser, R. S., Ferrare, R. A., Kaufman, Y. J., Markham, B. L., & Mattoo, S. (1992). Algorithm for atmospheric corrections of
525   aircraft and satellite imagery. International Journal of Remote Sensing, 13(3), 541-557.

Guo, J. P., Zhang, X. Y., Wu, Y. R., Zhaxi, Y., Che, H. Z., & Ba, L., et al. (2011). Spatio-temporal variation trends of satellite-based aerosol optical depth in China during 1980–2008. Atmospheric Environment,45(37), 6802-6811.

Guo, J., M. Deng, S. S. Lee, F. Wang, Z. Li, P. Zhai, H. Liu, W. Lv, W. Yao, and X. Li (2016). Delaying precipitation and lightning by air pollution over the Pearl River Delta. Part I: Observational analyses. Journal of Geophysical Research:
530   Atmospheres, 121, 6472–6488, doi:10.1002/2015JD023257.

Guo, J., Su, T., Li, Z., Miao, Y., Li, J., Liu, H., Xu, H., Cribb, M. and Zhai, P. (2017). Declining frequency of summertime local-scale precipitation over eastern China from 1970 to 2010 and its potential link to aerosols. Geophysical Research Letters, 44(11), 5700-5708.

He, Q., Zhang, M., & Huang, B. (2016). Spatio-temporal variation and impact factors analysis of satellite-based aerosol
535   optical depth over China from 2002 to 2015. Atmospheric Environment, 129, 79-90.

Holben, B. N., Eck, T. F., Slutsker, I., Tanre, D., Buis, J. P., Setzer, A., Vermote, E., Reagan, J.A., Kaufman, Y. J., Nakajima, T., Lavenu, F., Jankowiak, I., & Smirnov, A. (1998). AERONET – A federated instrument network and data archive for aerosol characterization. Remote Sensing of Environment, 66, 1–16.

Hollmann, R., C. Merchant, R. Saunders, C. Downy, M. Buchwitz, A. Cazenave, E. Chuvieco, P. Defourny, G. de Leeuw, R.
540   Forsberg, T. Holzer-Popp, F. Paul, S. Sandven, S., Sathyendranath, M. van Roozendael, W. Wagner (2013). The ESA
    climate change initiative: satellite data records for essential climate variables. Bulletin of the American Meteorological
    Society, 1541-1552.

Holzerpopp, T., Leeuw, G. D., Martynenko, D., & Klüser, L. (2013). Aerosol retrieval experiments in the esa aerosol_cci
    project. Atmospheric Measurement Techniques,6,8(2013-08-08), 6(8), 1919-1957.

545 Hsu, N. C., Jeong, M. -J., Bettenhausen, C., Sayer, A. M., Hansell, R., Seftor, C. S., . . . Tsay, S. -C. (2013). Enhanced deep
    blue aerosol retrieval algorithm: The second generation. Journal of Geophysical Research: Atmospheres, 118(16),
    9296–9315. doi:10.1002/jgrd.50712.

Hsu, N. C., Tsay, S. C., King, M. D., & Herman, J. R. (2004). Aerosol properties over bright-reflecting source regions. IEEE
    Transactions on Geoscience & Remote Sensing, 42(3), 557-569.

550 Hsu, N. C., Tsay, S. C., M.D. King, & Herman, J. R. (2006). Deep blue retrievals of Asian aerosol properties during ace-
    Asia. IEEE Transactions on Geoscience & Remote Sensing, 44(11), 3180-3195.

Ignatov, A., & Stowe, L. (2002). Aerosol retrievals from individual avhrr channels. part i: retrieval algorithm and transition
    from dave to 6s radiative transfer model. Journal of the Atmospheric Sciences, 59(59), 313-334.

Kaufman, Y. J., Wald, A. E., Remer, L. A., Gao, B. C., Li, R. R., & Flynn, L. (1997). The MODIS 2.1 mm channel
555   correlation with visible reflectance for use in remote sensing of aerosol, IEEE Transactions on Geoscience & Remote
    Sensing, 35(5), 1286-1298.

King, M. D., Kaufman, Y. J., Menzel, W. P., & Tanré, D. (1992). Remote sensing of cloud, aerosol, and water vapor
    properties from the moderate resolution imaging spectrometer (MODIS). IEEE Transactions on Geoscience & Remote
    Sensing, 30(1), 2-27.

560 Klingmueller, K., Pozzer, A., Metzger, S., Abdelkader, M., Stenchikov, G., & Lelieveld, J. (2016). Aerosol optical depth
    trend over the middle east. Atmospheric Chemistry & Physics, 16(8), 5063-5073.

Kalashnikova, O. V., Garay, M. J., Martonchik, J. V., and Diner, D. J. (2013). MISR Dark Water aerosol retrievals:
    operational algorithm sensitivity to particle non-sphericity, Atmospheric Measurement Techniques, 6, 2131–2154.

Kolmonen, P., Sogacheva, L., Virtanen, T.H., de Leeuw, G., and Kulmala, M. (2016). The ADV/ASV AATSR aerosol
565   retrieval algorithm: current status and presentation of a full-mission AOD data set. International Journal of Digital
    Earth, 9:6, 545-561

Levy, R. C., L. A. Remer, S. Mattoo, E. F. Vermote, and Y. J. Kaufman. (2007). Second generation operational algorithm:
    retrieval of aerosol properties over land from inversion of MODIS spectral reflectance. Journal of Geophysical
    Research Atmospheres,112, 1-21.

570 Levy, R. C., S. Mattoo, L. A. Munchak, L. A. Remer, A. M. Sayer, F. Patadia, and N. C. Hsu (2013), The Collection 6
    MODIS aerosol products over land and ocean, Atmos. Meas. Tech., 6, 2989–3034, doi:10.5194/amt-6-2989-2013.

Li, Z., Guo, J., Ding, A., Liao, H., Liu, J., & Sun, Y., et al. (2017). Aerosol and boundary-layer interactions and impact on air quality. National Science Review, 4 (6), 810–833. doi: 10.1093/nsr/nwx117.

Li, Z., Niu, F., Fan, J., Liu, Y., Rosenfeld, D., & Ding, Y. (2011). Long-term impacts of aerosols on the vertical development of clouds and precipitation. Nature Geoscience, *4*(12), 888–894. doi:10.1038/ngeo1313.

Martonchik, J. V. (1997). Determination of aerosol optical depth and land surface directional reflectances using multiangle imagery. Journal of Geophysical Research Atmospheres, 102(D14), 17015-17022.

Martonchik, J. V., & Diner, D. J. (1992). Retrieval of aerosol optical properties from multi-angle satellite imagery. IEEE Transactions on Geoscience & Remote Sensing, 30(2), 223 - 230.

Martonchik, J. V., Diner, D. J., Kahn, R. A., Ackerman, T. P., Verstraete, M. M., & Pinty, B., et al. (1998). Techniques for the retrieval of aerosol properties over land and ocean using multi-angle imaging. IEEE Transactions on Geoscience & Remote Sensing, 36(4), 1212-1227.

Martonchik, J. V., Kahn, R. A., and Diner, D. J. (2009). Retrieval of aerosol properties over land using MISR observations, in: Satellite Aerosol Remote Sensing of Land, edited by: Kokhanovsky, A. A.and de Leeuw, G., Springer, Berlin, 267–293, doi:10.1007/978-3-540-69397-0_9.

Mehta, M., Singh, R., Singh, A., Singh, N., & Anshumali. (2016). Recent global aerosol optical depth variations and trends — a comparative study using modis and misr level 3 datasets. Remote Sensing of Environment,181, 137-150.

North, P. R. J. (2002). Estimation of aerosol opacity and land surface bidirectional reflectance from atsr-2 dual-angle imagery: operational method and validation. Journal of Geophysical Research Atmospheres,107(D12), AAC-1-AAC 4-10.

North, P. R. J., Briggs, S. A., Plummer, S. E., & Settle, J. J. (1999). Retrieval of land surface bidirectional reflectance and aerosol opacity from atsr-2 multiangle imagery. IEEE Transactions on Geoscience & Remote Sensing, 37(1), 526-537.

Pöschl, U. (2005). Atmospheric aerosols: composition, transformation, climate and health effects. Cheminform, 44(46), 7520-7540.

Poulsen, C. A., Siddans, R., Thomas, G. E., Sayer, A. M., Grainger, R. G., & Campmany, E., et al. (2012). Cloud retrievals from satellite data using optimal estimation: evaluation and application to atsr. Atmospheric Measurement Techniques, 5(8), 1889-1910.

Popp, T., de Leeuw, G., Bingen, C., Brühl, Christoph, Capelle, V., Chedin, A., Clarisse, L., Dubovik, O., Grainger, R., Griesfeller, J., Heckel, A., Kinne, S., Klüser, L., Kosmale, M., Kolmonen, P., Lelli, L., Litvinov, P., Mei, L., North, P., Pinnock, S., Povey, A., Robert, C., Schulz, M., Sogacheva, L., Stebel, K., Stein Zweers, D., Thomas, G., Tilstra, L.G., Vandenbussche, S., Veefkind, P., Vountas, M., and Xue, Y. (2016). Development, production and evaluation of aerosol Climate Data Records from European satellite observations (Aerosol_cci). Remote Sensing. 2016, 8, 421; doi:10.3390/rs8050421.

Ramanathan, V., Crutzen, P. J., Kiehl, J. T., and Rosenfeld, D.: Aerosols, climate and the hydrological cycle, Science, 294, 2119–2124, 2001.

Rosenfeld, D., Lohmann, U., Raga, G. B., O'Dowd, C. D., Kulmala, M., Fuzzi, S., Reissell, A., and Andreae, M. O.: Flood or drought: How do aerosols affect precipitation?, Science, 321, 1309–1313, doi:10.1126/science.1160606, 2008

Sayer, A. M., Hsu, N. C., Bettenhausen, C., Ahmad, Z., Holben, B. N., & Smirnov, A., et al. (2012). Seawifs ocean aerosol retrieval (soar): algorithm, validation, and comparison with other data sets. Journal of Geophysical Research

610   Atmospheres, 117(D3), -.

Sayer, A.M., Poulsen, C. A., Arnold, C., Campmany, E., Dean, S., Ewen, G. B.L., et al. (2011). Global retrieval of ATSR cloud parameters and evaluation (GRAPE): dataset assessment. Atmospheric Chemistry and Physics, 11, 3913–3936. http://dx.doi.org/10.5194/acp-11-3913-2011

Sogacheva, L., de Leeuw, G., Rodriguez, E., Kolmonen, P., Georgoulias, A. K., Alexandri, G., Kourtidis, K., Proestakis, E.,

615   Marinou, E., Amiridis, V., Xue, Y., and van der A, R. J.: Spatial and seasonal variations of aerosols over China from two decades of multi-satellite observations – Part 1: ATSR (1995–2011) and MODIS C6.1 (2000–2017), Atmos. Chem. Phys., 18, 11389-11407.

Stowe, L. L., A. M. Ignatov, and R. R. Sigh (1997), Development, validation, and potential enhancements to the second-generation operational aerosol product at the National Environmental Satellite, Data, and Information Service of the

620   National Oceanic and Atmospheric Administration, Journal of Geophysical Research, 102, 16,923–16,932

Sun, L., Wei, J., Bilal, M., Tian, X., Jia, C., & Guo, Y., et al. (2016). Aerosol optical depth retrieval over bright areas using Landsat 8 OLI images. Remote Sensing, 8(1), 23.

Thomas, G. E., Poulsen, C. A., Sayer, A.M., Marsh, S. H., Dean, S. M., Carboni, E., et al. (2009). The GRAPE aerosol retrieval algorithm. Atmospheric Measurement Techniques, 2, 679–701. http://dx.doi.org/10.5194/amt-2-679-2009.

625 Veefkind, J. P., & Leeuw, G. D. (1998). A new algorithm to determine the spectral aerosol optical depth from satellite radiometer measurements. Journal of Aerosol Science, 29(10), 1237-1248.

Wei, J., & Sun, L. (2017). Comparison and evaluation of different MODIS aerosol optical depth products over the Beijing-Tianjin-Hebei region in china. IEEE Journal of Selected Topics in Applied Earth Observations & Remote Sensing, 10(3):835-844

630 Wei, J., Huang, B., Sun, L., Zhang, Z., Wang, L., & Bilal, M. (2017). A simple and universal aerosol retrieval algorithm for Landsat series images over complex surfaces. Journal of Geophysical Research Atmospheres,122(24) 22(24):13338-13355

Wei, J., Sun, L., Huang, B., Bilal, M., Zhang, Z., & Wang, L. (2018). Verification, improvement and application of aerosol optical depths in China part 1: Inter-comparison of NPP-VIIRS and Aqua-MODIS. Atmospheric Environment, 175,

635   221-233.

Xin, J., Wang, Y., Li, Z., Wang, P., Hao, W. M., & Nordgren, B. L., et al. (2007). Aerosol optical depth (AOD) and angstrom exponent of aerosols observed by the Chinese Sun Hazemeter network from august 2004 to September 2005. Journal of Geophysical Research Atmospheres, 112(D5), 1703-1711.

Zhao, X. P., Dubovik, O., Smirnov, A., Holben, B. N., Sapper, J., & Pietras, C., et al. (2004). Regional evaluation of an
640   advanced very high resolution radiometer (AVHRR) two-channel aerosol retrieval algorithm. Journal of Geophysical
     Research Atmospheres, 109(D2), -.

Zhao, X. P., Laszlo, I., Guo, W., Heidinger, A., Cao, C., & Jelenak, A., et al. (2008). Study of long-term trend in aerosol
     optical thickness observed from operational AVHRR satellite instrument. Journal of Geophysical Research
     Atmospheres, 113(D7), -.

645 Zhao, X.-P, T., Chan, & Pui, K. (2013). A global survey of the effect of cloud contamination on the aerosol optical thickness
     and its long-term trend derived from operational AVHRR satellite observations. Journal of Geophysical Research
     Atmospheres, 118(7), 2849-2857.

650 Table 1. Summary of satellite data sources used in this study

Product	Scientific Data Set (SDS) name	Version/ Collection	Spatial resolution	Period
AATSR-ADV	AOD550_mean	V2.31	1°×1°	1996.07-2012.04
AATSR-SU	AOD550_mean	V4.3	1°×1°	1996.07-2012.04
AATSR-ORAC	AOD550_mean	V4.01	1°×1°	1996.07-2012.04
AATSR-EN	AOD550	V2.6	1°×1°	1996.07-2012.04
AVHRR	aot1	-	0.1°×0.1°	1997.01-2017.12
MISR	Optical depth average (550 nm)	V23	0.5°×0.5°	2000.02-2017.05
MOD08	AOD_550_Dark_Target_Deep_Blue_Combined_Mean	C6.1	1°×1°	2000.02-2017.12
MYD08	AOD_550_Dark_Target_Deep_Blue_Combined_Mean	C6.1	1°×1°	2002.07-2017.12
SeaWiFS	aerosol_optical_thickness_550_land	V004	0.5°×0.5°	1997.09-2010.12
AERONET	AOD at 550 nm	V3	-	1996.07-2017.12

655

Table 2. Validation statistics for operational aerosol products over land and ocean during the common period

Products	Land (2003-2010)				Ocean (2003-2010)			
Metrices	N	MAE	RMSE	= EE	N	MAE	RMSE	= EE
AATSR-ADV	9939	0.081	0.139	69.55	1550	0.062	0.084	66.71
AATSR-EN	10801	0.078	0.133	70.99	1636	0.054	0.073	74.14
AATSR-ORAC	11530	0.077	0.130	70.15	1653	0.065	0.084	62.61
AATSR-SU	10483	0.078	0.138	71.42	1594	0.051	0.074	77.98
AVHRR	-	-	-	-	1649	0.057	0.079	73.38
MISR	**11707**	0.076	0.122	68.59	1682	0.061	0.086	69.98
MOD08	11432	0.072	0.107	68.54	1723	0.065	0.083	63.38
MYD08	11175	**0.065**	**0.104**	**74.97**	**1723**	**0.050**	**0.067**	**78.29**
SeaWiFS	7282	0.079	0.128	69.29	1153	0.050	0.071	78.06

660   Table 3. Statistics of annual mean AOD biases among different aerosol products from 2003 to 2010

Products	ENAM	NSAM	EUR	NAF	ME	SAA	EAA	Land	Ocean
ADV	0.014	0.012	-0.029	-0.139	-0.051	-0.068	-0.078	-0.026	0.030
EN	0.023	-0.013	-0.009	-0.048	0.062	-0.078	-0.121	-0.01	0.017
ORAC	0.042	-0.064	-0.002	-0.173	-0.021	-0.141	-0.129	-0.023	0.044
SU	0.022	0.054	-0.012	0.025	0.081	-0.054	-0.109	0.009	-0.004
MISR	-0.007	-0.065	-0.025	-0.095	0.035	-0.112	-0.171	-0.034	0.018
MOD08	0.049	0.023	0.038	-0.035	0.088	0.108	0.067	0.035	0.054
MYD08	0.032	0.003	0.015	-0.033	0.066	0.069	0.057	0.019	0.035
SeaWiFS	-0.013	-0.152	-0.026	-0.055	-0.03	-0.014	-0.176	-0.036	0.008
AVHRR	-	-	-	-	-	-	-	-	-0.031
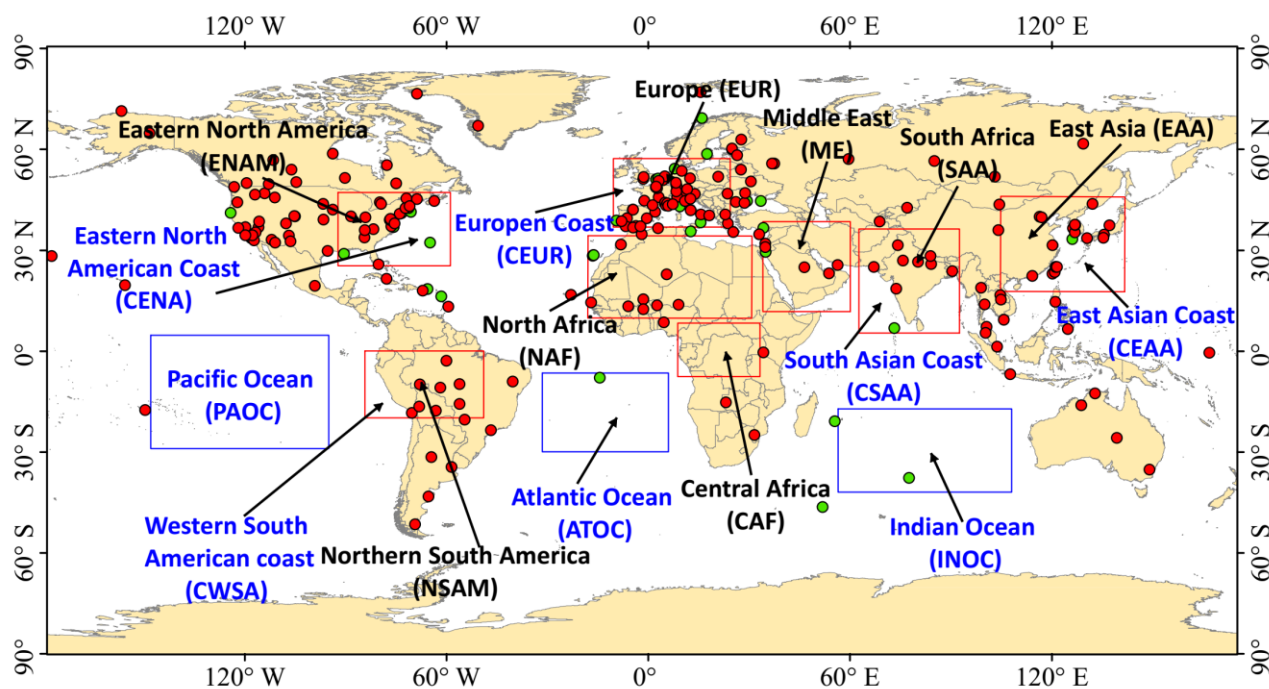
Figure 1. Locations of AERONET sites and geographical bounds of custom regions used in this study, where red and green
dots represent land and ocean sites, and black and blue annotations represent land and ocean regions. The three ocean
regions with blue frames indicate open ocean areas far from continental aerosol sources.
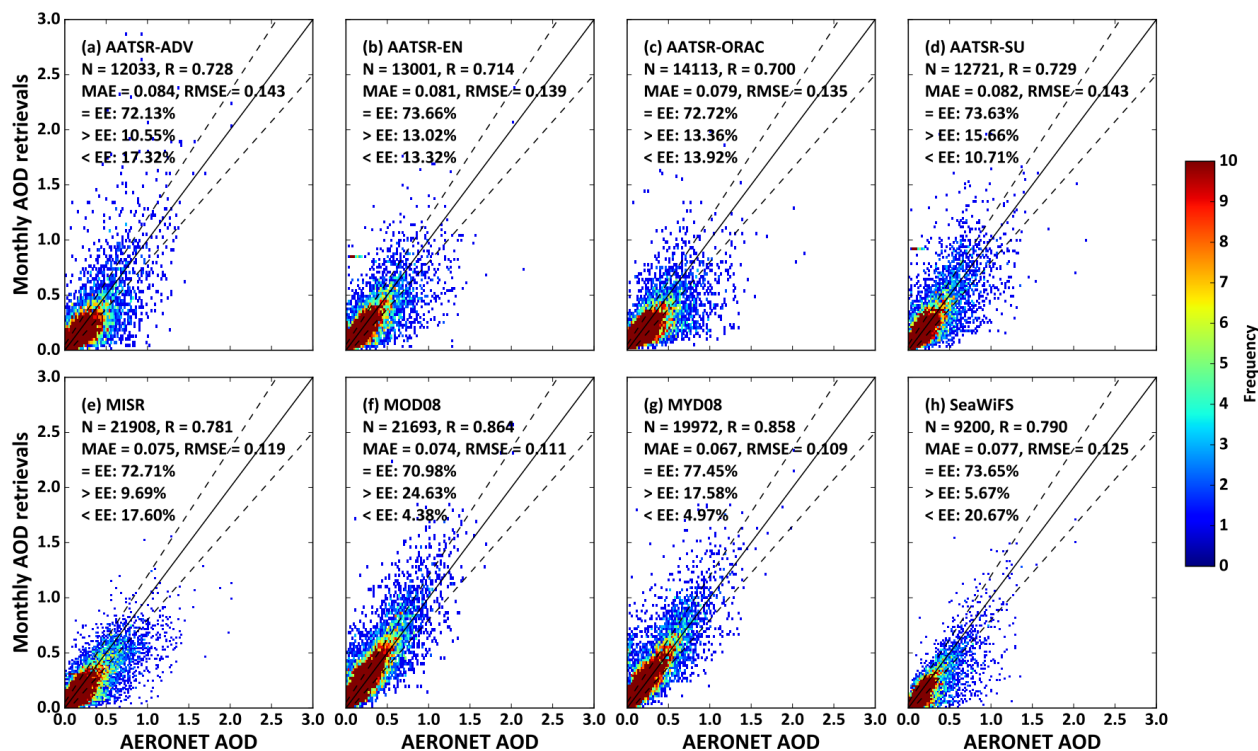
Figure 2. Density scatters of operational aerosol products against AERONET AOD measurements over land.

670
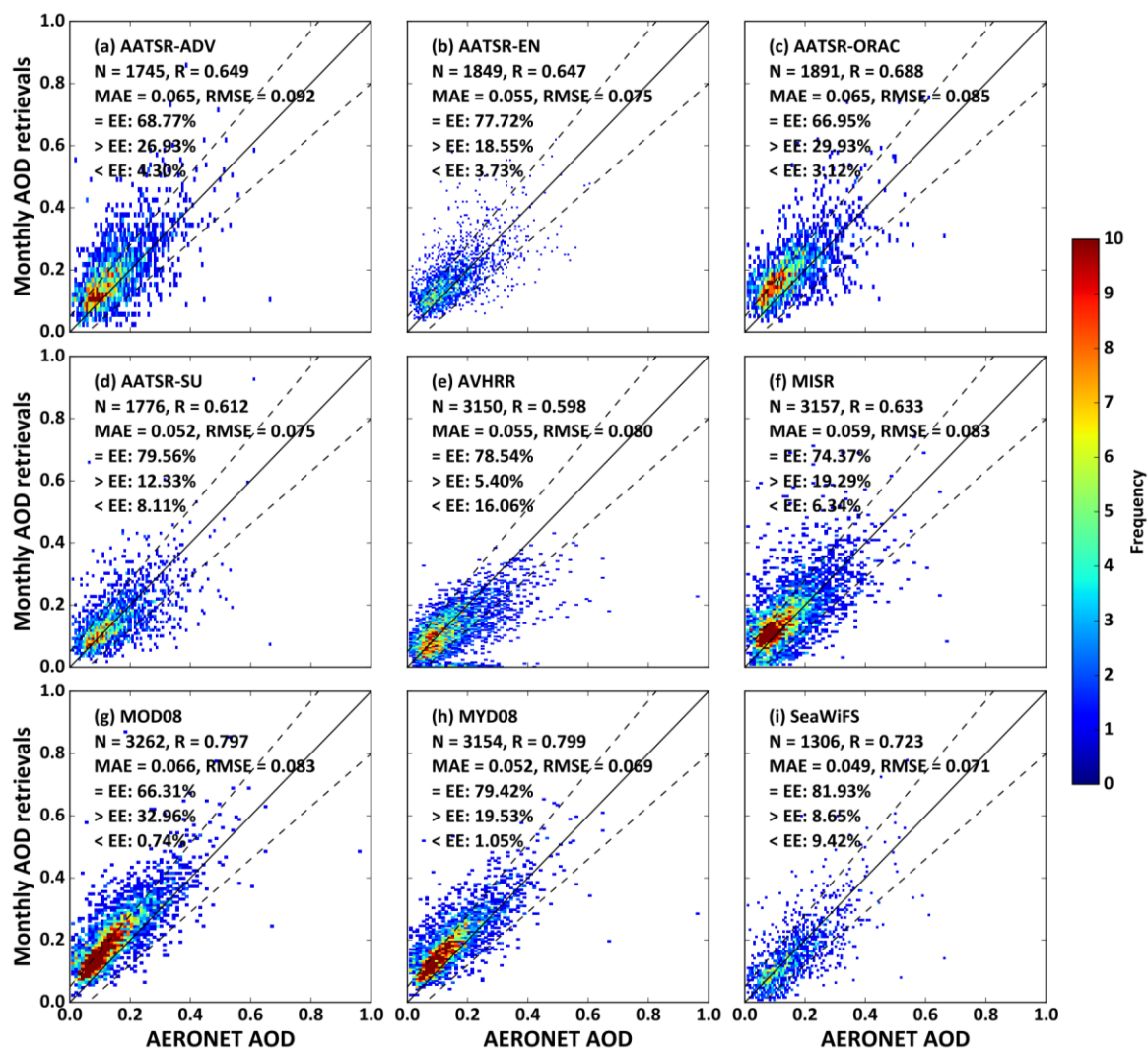
Figure 3. Density scatters of operational aerosol products against AERONET AOD measurements over the ocean.
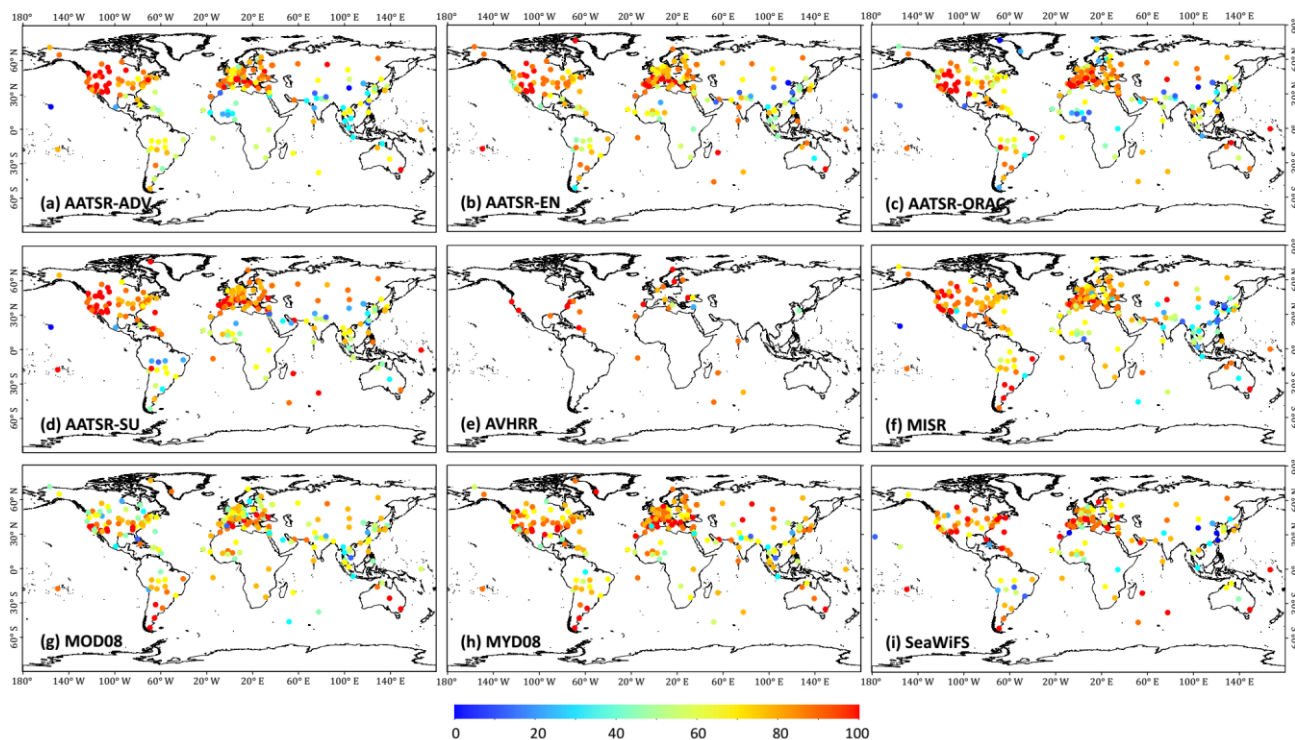
675   Figure 4. Site performance map for the percentage (*f*) of retrievals within the EE (=EE, %) among nine operational aerosol

products. Each of the selected AERONET sites must have at least 2 years ground-based monthly observations (at least 24

matchups).
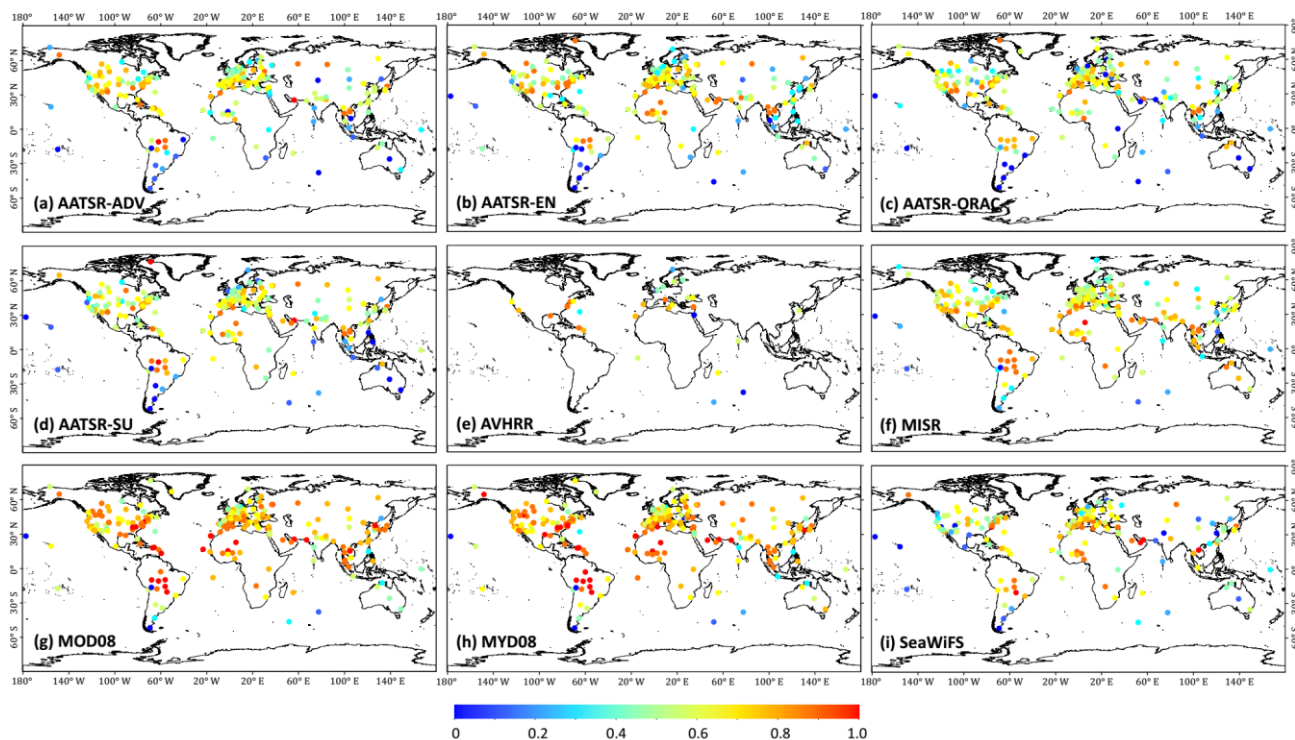
Figure 5. Similar to Figure 4 but for the correlation coefficient (R)
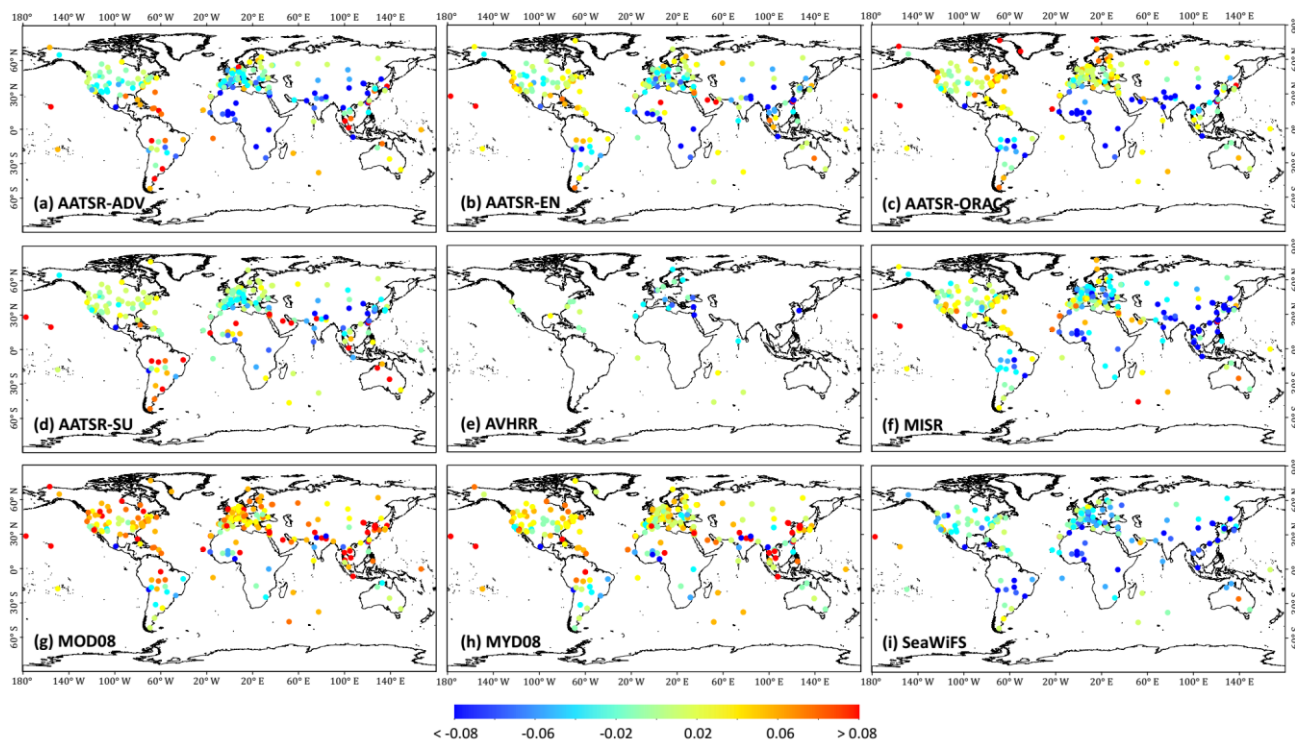
Figure 6. Similar to Figure 4 but for mean bias (MB)
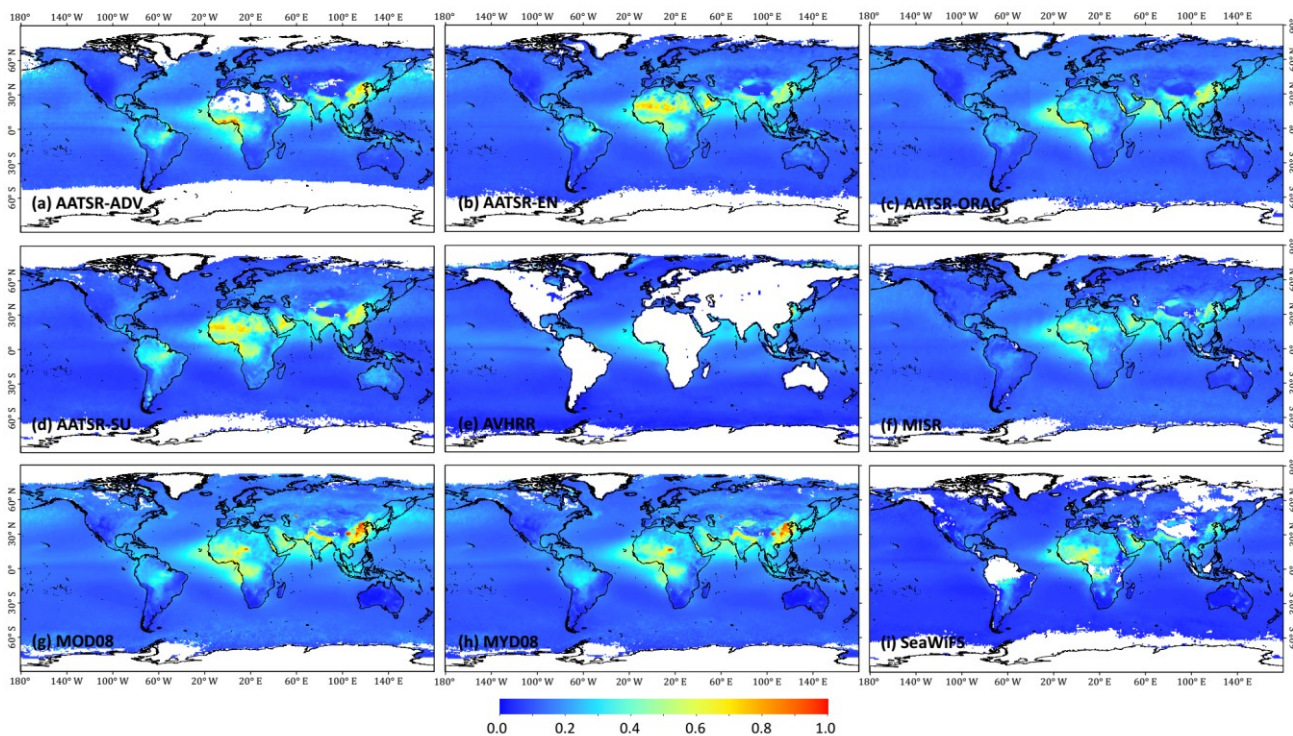
685

Figure 7. Spatial distributions of annual mean aerosols over land and ocean from 2003 to 2010.
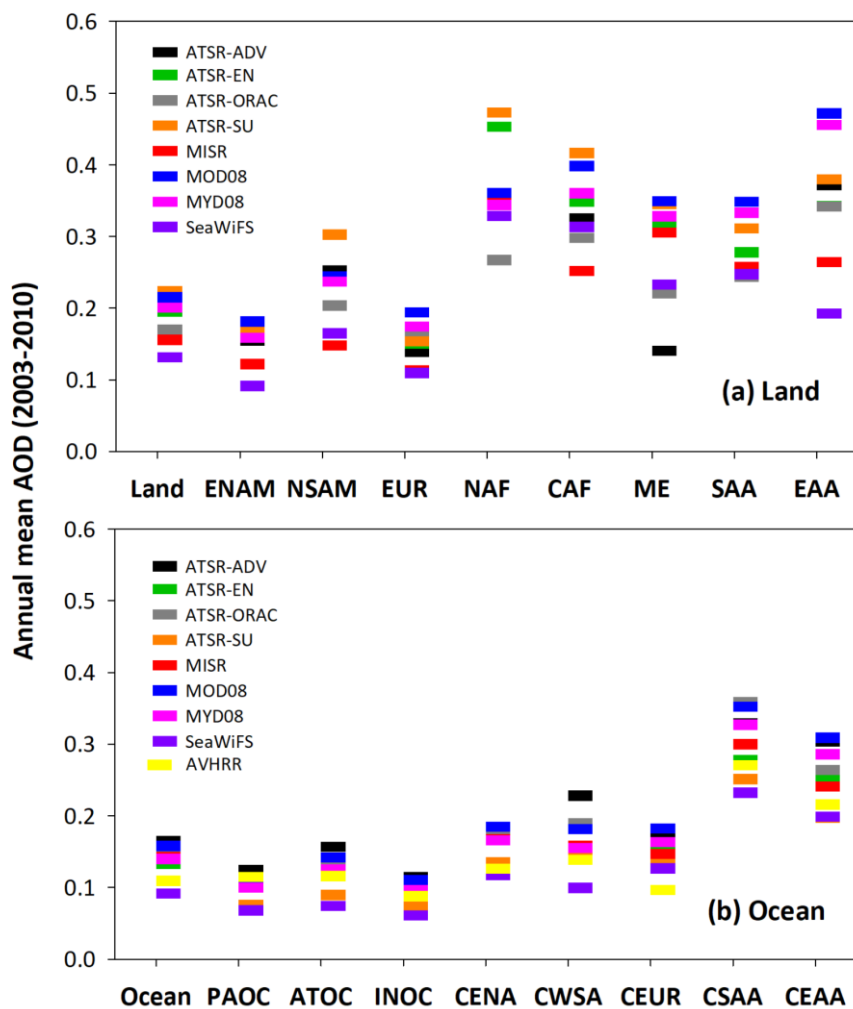
Figure 8. Distributions of annual mean aerosols over land and ocean from 2003 to 2010.

690
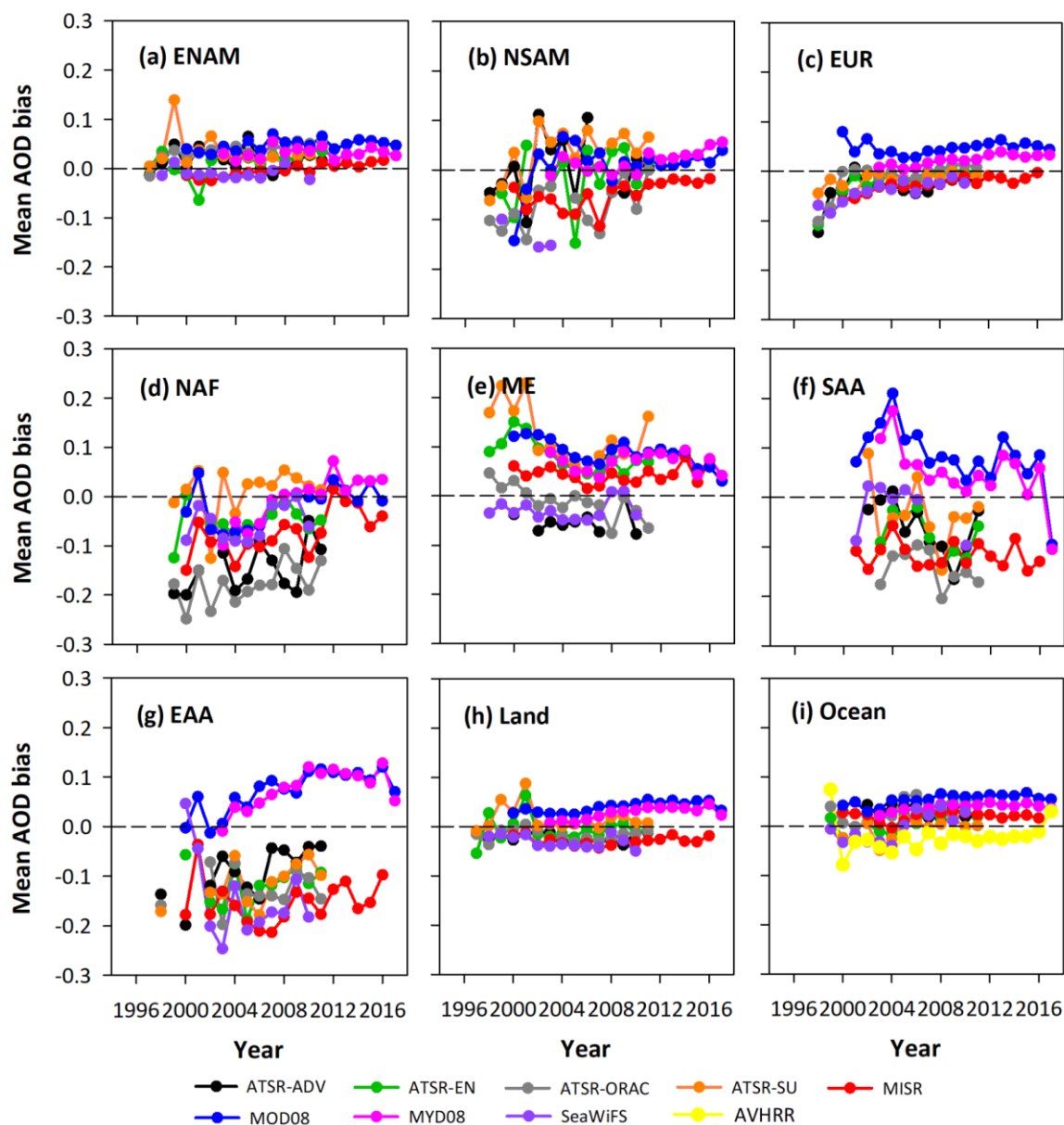
Figure 9. Mean bias between satellite-derived and AERONET measured annual mean AODs over time over land and ocean.
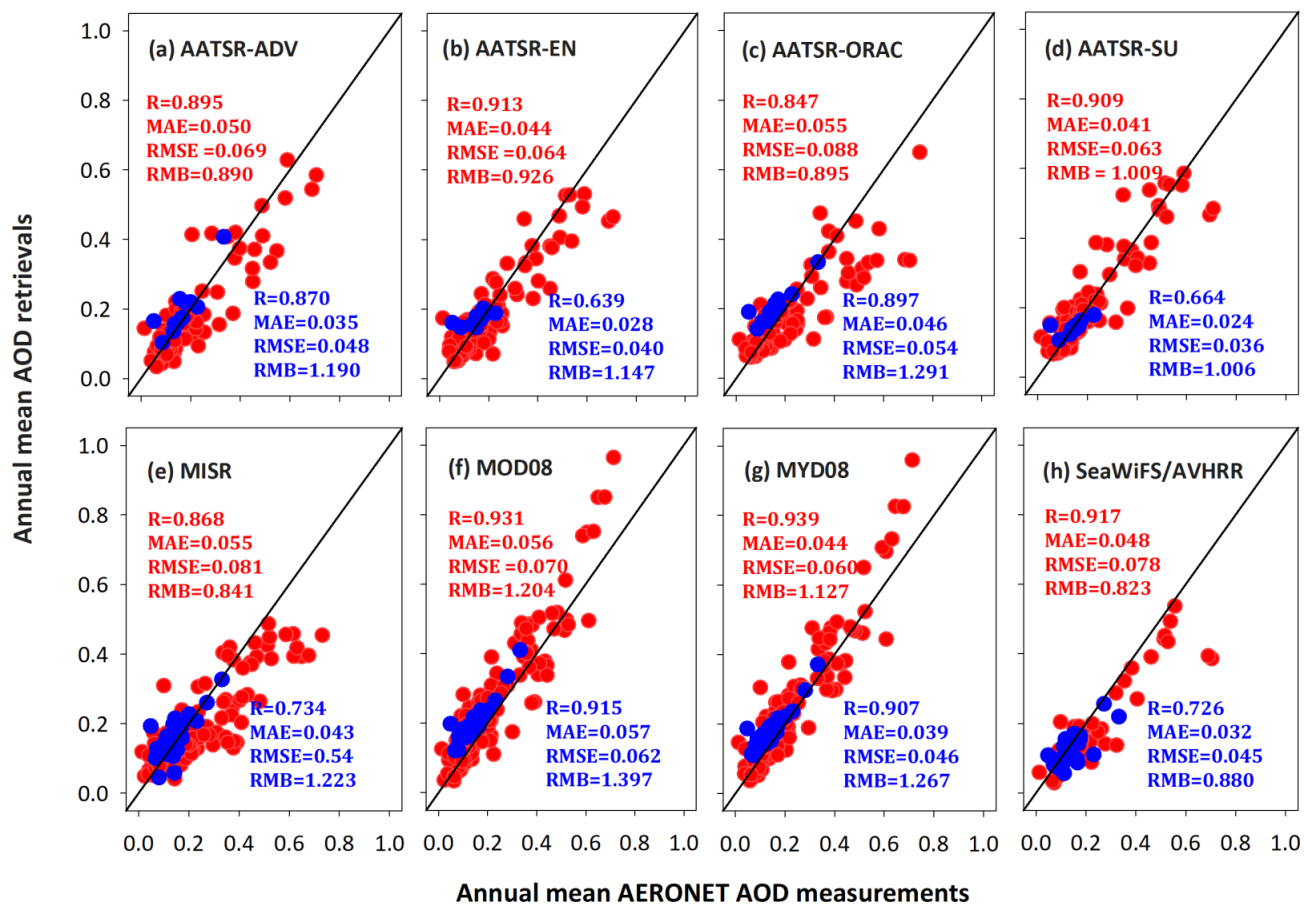
Figure 10. Validation of annual mean AODs by comparing with AERONET AOD measurements among all aerosol datasets
695   for all sites over land (red dots) and ocean (blue dots). The solid black line represents the 1:1 line.
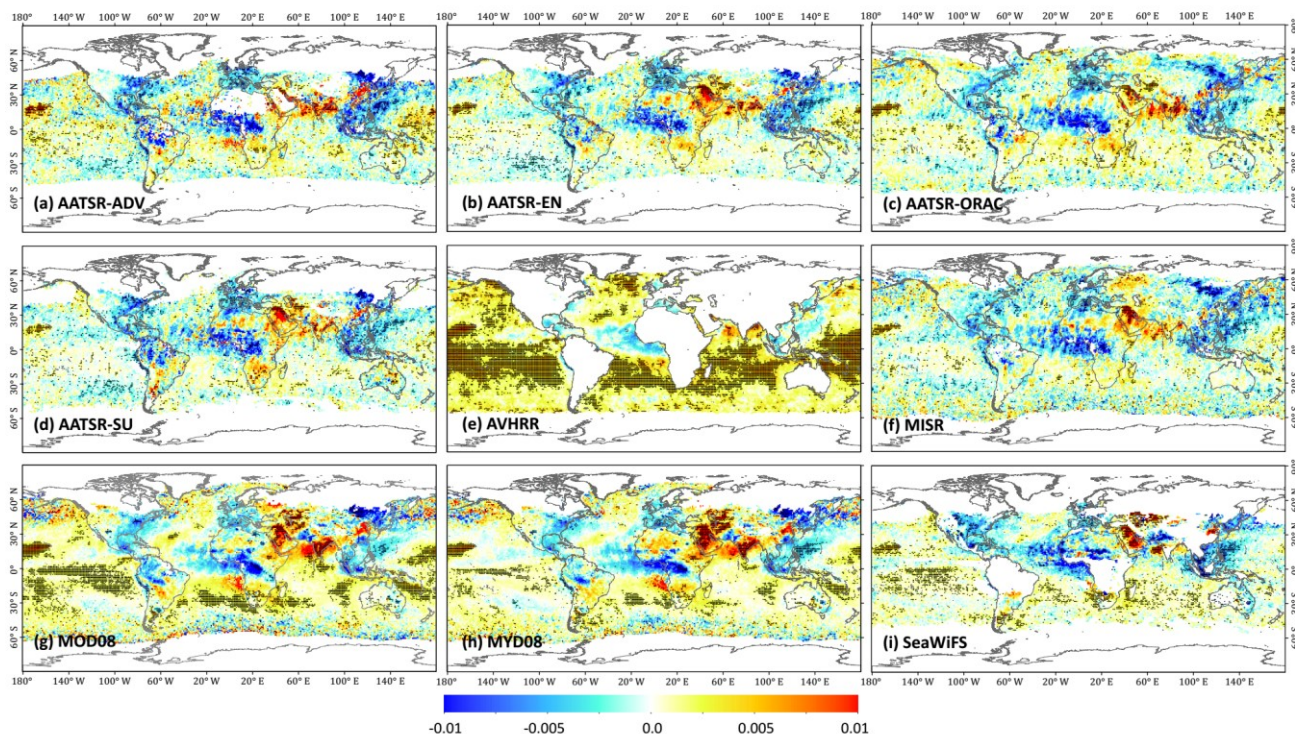
Figure 11. Spatial distributions of AOD trends at 550 nm for nine operational aerosol products over land and ocean from 2003 to 2017, where the black spots indicate that trend is significant at the 95% confidence level (p<0.05)
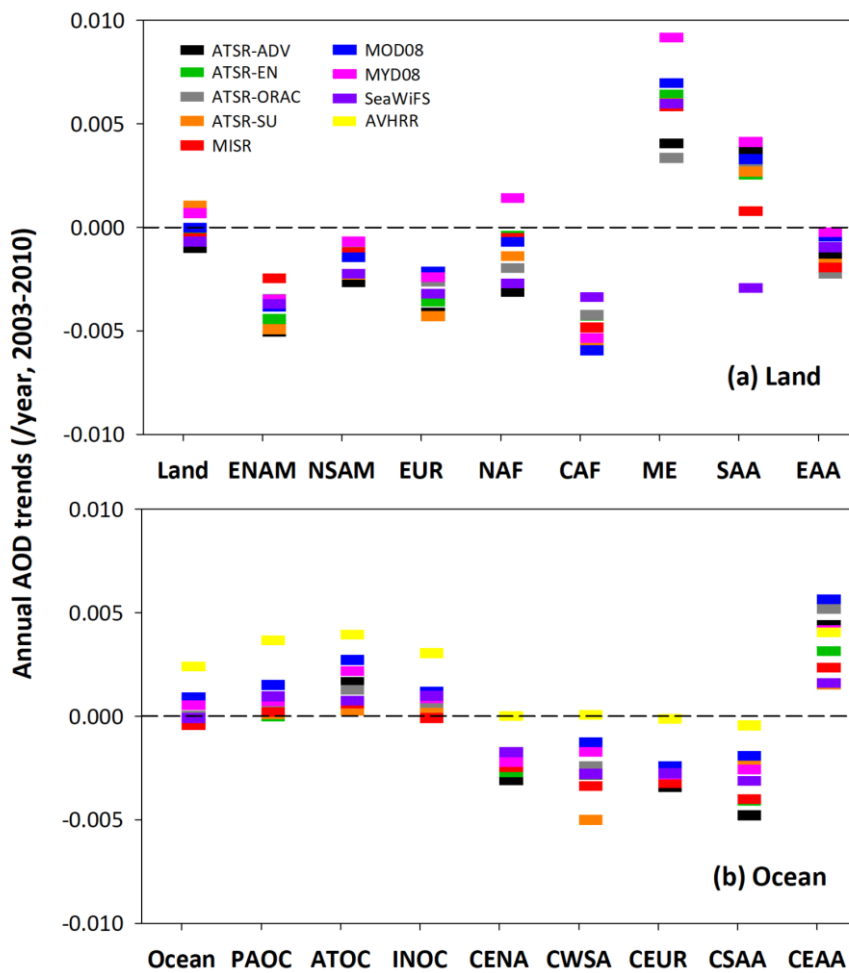
700   Figure 12. Numerical distributions of aerosol trends over land and ocean from 2003 to 2010.
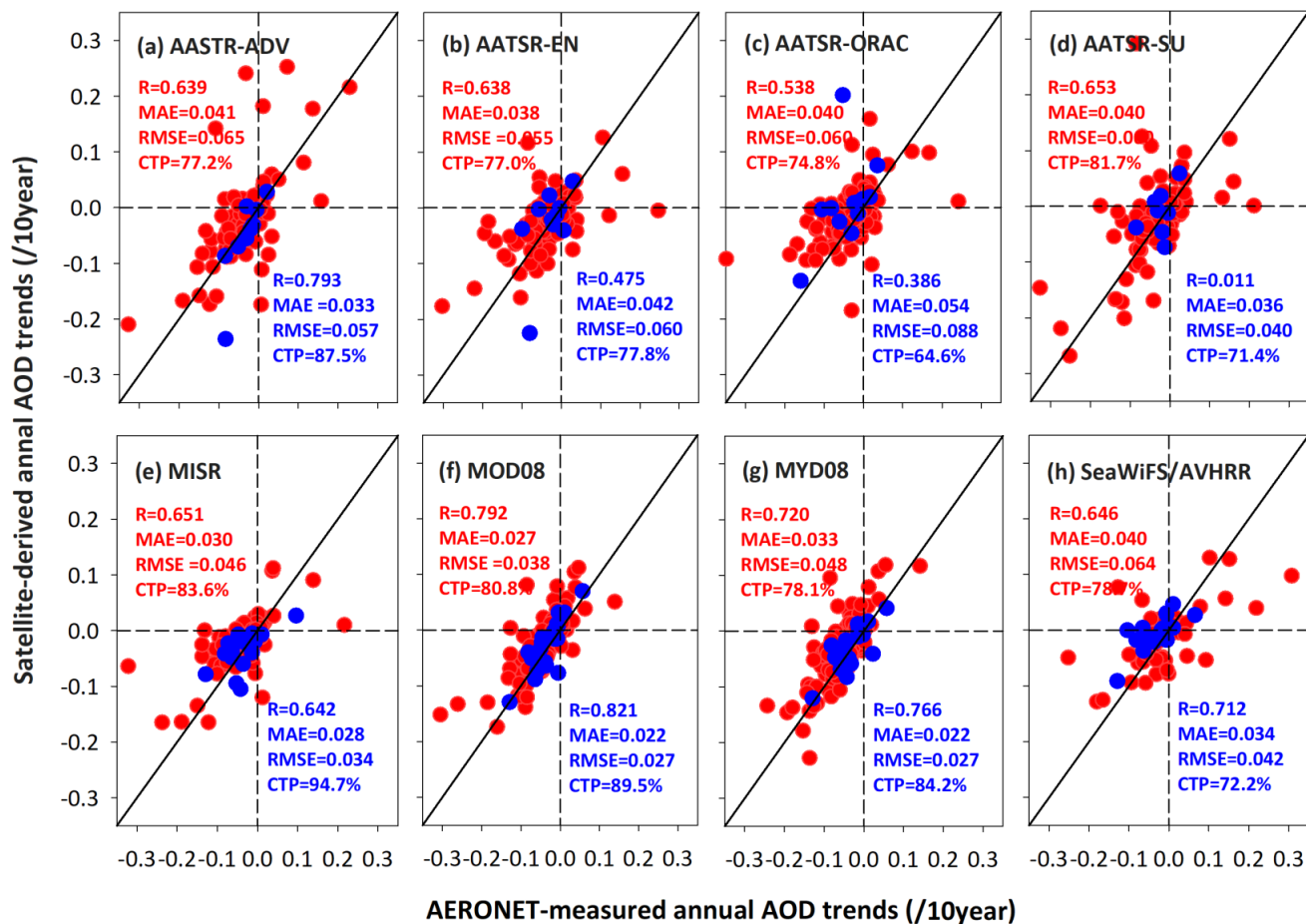
Figure 13. Distributions of annual mean aerosols over land and ocean from 2003 to 2010.
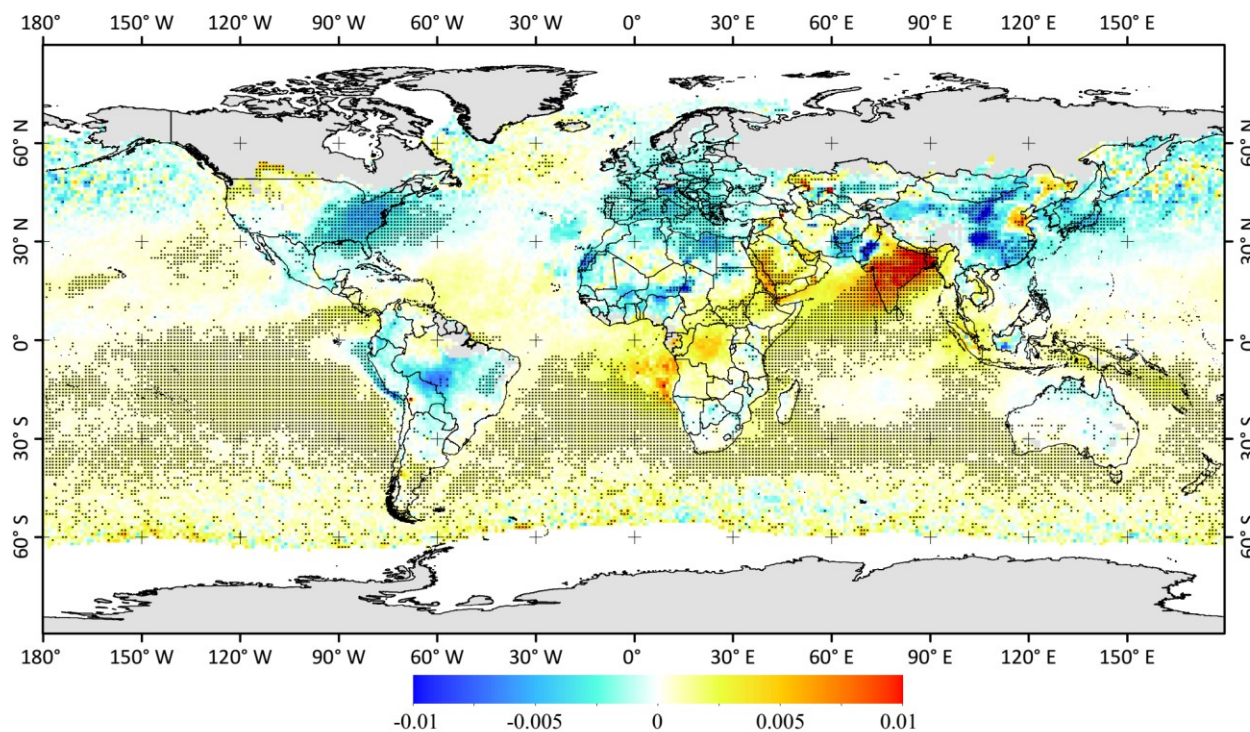
Figure 14. Annual aerosol trends (yr⁻¹) based upon deseasonalized monthly anomaly Terra MODIS AOD at 550 nm for the
period 2000–2017. Units are AOD yr-1. Dots indicate significance at 95 % confidence level. Regions shaded in grey indicate
no data or insufficient sample size for trend analysis.
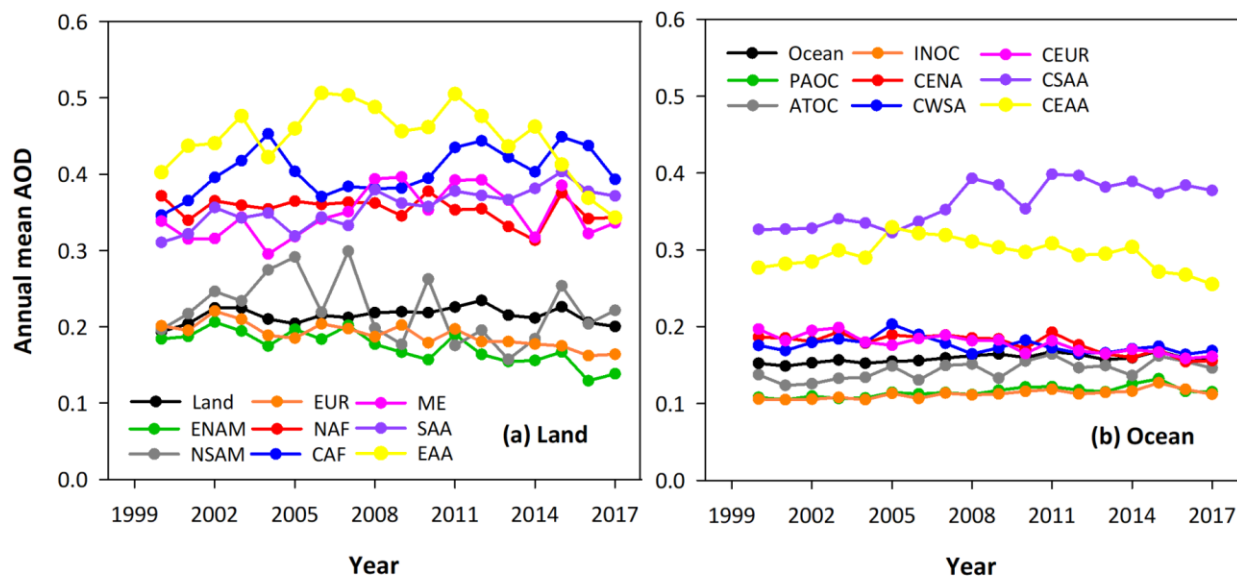
Figure 15. MODIS time series of annual mean AOD variations over land (a) and ocean (b) from 2000 to 2017.